Elucidating the role of NiMoS-USY during the hydrotreatment of Kraft lignin

Chemical Engineering Journal 442 (2022) 136216

Contents lists available at ScienceDirect

Chemical Engineering Journal

journal homepage: www.elsevier.com/locate/cej

Elucidating the role of NiMoS-USY during the hydrotreatment of Kraft lignin

Muhammad Abdus Salam [a], You Wayne Cheah [a], Phuoc Hoang Ho [a], Diana Bernin [b], Abdenour Achour [a], Elham Nejadmoghadam [a], Olov Öhrman [c], Prakhar Arora [c], Louise Olsson [a], Derek Creaser [a,*]

[a] Chemical Engineering, Competence Centre for Catalysis, Chalmers University of Technology, SE-412 96 Gothenburg, Sweden
[b] Department of Chemistry and Chemical Engineering, Chalmers University of Technology, SE-412 96 Gothenburg, Sweden
[c] Preem AB, Sweden

ARTICLE INFO

Keywords:
NiMo
USY
Kraft lignin
Depolymerization
Hydrodeoxygenation
Reductive liquefaction

ABSTRACT

Major hurdles in Kraft lignin valorization require selective cleavage of etheric and C–C linkages and subsequent stabilization of the fragments to suppress repolymerization reactions to yield higher monomeric fractions. In this regard, we report the development of efficient NiMo sulfides and ultra-stable Y zeolites for the reductive liquefaction and hydrodeoxygenation of Kraft lignin in a Parr autoclave reactor at 400 °C and 35 bar of H_2 (@25 °C). Comparing the activity test without/with catalyst, it is revealed that NiMo sulfides over ultra-stable Y zeolites (silica/alumina = 30) achieved a significant reduction (~50 %) of the re-polymerized solid residue fraction leading to a detectable liquid product yield of 30.5 wt% with a notable monocyclic and alkylbenzenes selectivity (~61 wt%). A physical mixture counterpart, consisting of hydrothermally synthesized unsupported NiMoS and Y30, on the other hand, shows lower selectivity for such fractions but higher stabilization of the lignin fragments due to enhanced access to the active sites. Moreover, an extended reaction time with higher catalyst loading of the impregnated NiMoY30 facilitated a remarkable alkylbenzene (72 wt%) selectivity with an increased liquid yield of 38.9 wt% and a reduced solid residue of 16.4 wt%. The reason for the high yield and selectivity over NiMoY30, according to the catalyst characterization (H_2-TPR, XPS, TEM) can be ascribed to enhanced stabilization of depolymerized fragments via H_2-activation at a lower temperature and high hydrodeoxygenation ability. In addition, the better proximity of the acidic and deoxygenation sites in NiMoY30 was beneficial for suppressing the formation of polycyclic aromatics.

1. Introduction

Lignin, a naturally abundant renewable raw material, has been exploited in current research to derive bio-based green chemicals and fuels due to growing environmental and political concerns [1]. Naturally, it is composed of phenylpropane units connected via irregular etheric and C–C linkages [2,3]. During the pulping/delignification process, full or partial breakdown of the labile etheric linkages makes the native lignin structure more intractable. The resulting product is often termed as technical lignin e.g., Kraft/lignosulfonate lignin [1]. To avoid these changes in the lignin structure, a reductive lignin-first biorefinery approach has been suggested [4,5]. However, even in its natural form lignin contains some recalcitrant interunit C–C linkages that can limit its conversion to monomer units. A successful transformation, therefore, necessitates the cleavage of both C-O and C–C linkages, stabilization, and upgradation of the monomeric fragments [6].

Various thermal, oxidative, reductive, acidic/alkaline, and catalytic processes have been explored for depolymerization/upgradation of Kraft lignin to bio-oil containing alkyl or methoxy substituted phenols, monocyclics/aromatics with residual solid, and coke formation [7,8]. The catalytic reductive liquefaction techniques, in which hydrodeoxygenation (HDO) reactions can be involved, have received rising interest and have been extensively explored using heterogeneous catalysts in single pot and multi-step processes [6,9,10]. In a typical one-pot thermochemical catalytic process, depolymerization, stabilization, and upgradation occur in tandem, and the catalyst employed plays a challenging pivotal role to fortify the yield of monomeric fractions with minimal formation of re-polymerized/condensed solid char fractions.

* Corresponding author.
E-mail address: creaser@chalmers.se (D. Creaser).

https://doi.org/10.1016/j.cej.2022.136216
Received 30 January 2022; Received in revised form 26 March 2022; Accepted 3 April 2022
Available online 5 April 2022

Nevertheless, solid residues or char formation can deactivate the catalysts prematurely [10]. Moreover, the presence of impurities such as alkali metals and sulfur in such feedstocks may pose additional difficulties in their upgradation and thus limit the number of suitable catalysts [11]. Particularly, the presence of sulfur (1–3 wt%) [7] can be strongly detrimental to the effectiveness of many noble metal-based solid catalysts (e.g., Pt, Ru, Pd, etc.). Since lignin has a high oxygen content (~30 wt%), the reductive process typically generates water via HDO, dehydration, and the reverse water gas shift reactions [12]. Hence the stability of the catalysts in the presence of a large amount of water is also crucial. An ideal/robust/stable catalyst shall thus be able to cleave lignin linkages, promote deoxygenation reactions and be tolerant of impurities and water while suppressing undesired side reactions. In this context, the current contribution illustrates the roles of NiMo sulfides and ultra-stable Y zeolites for the reductive liquefaction and hydrodeoxygenation of Kraft lignin in a one pot process to advanced biofuel components.

Being sulfur tolerant, classical Ni/Co-promoted Mo/W sulfides in supported or unsupported form have high HDO activity for the conversion of lignin derived methoxy/alkyl phenols to arenes and cycloalkanes [13–21]. They have also been found effective in cleaving both etheric and C–C linkages of lignin dimers [22–26]. Other transition metal sulfides (e.g FeS_2, VS_2, ReS_2) have also been reported as highly active for conversion of lignin and lignin surrogates [27–29]. High hydrogenolysis and HDO activity of the sulfided catalyst is typically governed by promoter/sulfur-vacancy engineering, tailoring the morphology of the layered structure and tuning textural properties obtained by varying the synthesis method [30]. It is important to note that during HDO process oxygenate molecules/in-situ generated water can influence the activity of sulfided catalysts via competitive adsorption and sulfur-oxygen exchange. However, the presence of sulfur in the feedstock or an added sulfur source (e.g., dimethyl disulfide, H_2S) can maintain the catalytic activity [31].

Sulfided catalysts with tailored properties have also been studied for lignin valorization. Hydrolysis lignin over a commercial sulfided $NiMoP/Al_2O_3$ has been exemplified to be valorized to paraffin, naphthenes, and aromatics in a semi-continuous tubular reactor, although with considerable solid residue (~20 wt%) formation, after 4 h of reaction at 380 °C and 40 bar of H_2 [12]. An increasing catalyst amount, pressure, and temperature were shown to favor the stabilization of intermediate fragments, HDO, and hydrocracking reactions respectively. Pu et al. [32] demonstrated an intriguing semi-continuous setup for lignin hydroconversion over a commercial sulfided $CoMo/Al_2O_3$ with a continuous H_2 supply. Mukundan et al.[33,34] reported thermocatalytic conversion of waste/Kraft lignin to oxygenated/deoxygenated aromatics at atmospheric and higher H_2 pressure. Solvent-free hydropyrolyis/hydrotreatment of Kraft lignin (395–400 °C, 100 bar of initial H_2 pressure, 0.3–0.6 h) has been reported with sulfided NiMo/aluminosilica and 20 wt% Cr_2O_3/Al_2O_3 to yield low solid residues (0–12 wt%) [35,36]. NiMo and CoMo sulfide catalysts over various acidic/basic supports were also explored, and $NiMo/MgO\text{-}La_2O_3$ was found to provide a better yield (26.4 wt%) of monomeric products [37]. In a hydrogen donor solvent, a sulfided NiW/AC catalyst was reported to yield 35 wt% of monomeric products (320 °C and 35 bar H_2, 24 h) with minimal char formation but with heavier DMSO (dimethylsufoxide) and DCM (dichloromethane) soluble fractions [11]. Liu et al. used lignosulfonate lignin as precursors for metal sulfide synthesis and reported 84% selectivity for 4-propylguaiacol upon depolymerization of lignosulfonate lignin in water over Co_3S_4/C [38]. Unsupported composite catalysts, NiS_2/MoS_2, and CoS_2/MoS_2 reportedly produced > 85% of bio-oil, with ~ 9 % solid residue, via depolymerization of alkali lignin at 310 °C, 25 bar of H_2 during 1 h using ethanol as solvent [39]. Thus, the choice of solvent, physicochemical properties of the support, and operation conditions in addition to the type of transition metal sulfides used play a crucial role in valorizing lignin. In this context, we examined here the role of NiMo sulfides over a series of acidic ultra-stable Y zeolites for Kraft lignin valorization using a non-polar solvent, hexadecane which is commonly available in a fuel refinery.

Ultra-stable Y zeolites rather than pristine Y-zeolite were chosen due to their large pore size, tunable acidity, and higher thermal and hydrothermal stability [40–42]. Also, USY zeolites have been used as stand-alone or modified solid acid catalysts for catalytic fast pyrolysis/liquefaction of biomass/Kraft lignin to obtain aromatics/deoxygenated products [40,43–47]. Earlier works from our group have shown that the combination of NiMo sulfides and Y zeolites can effectively catalyze both the cleavage of C-O-C and C–C linkages present in lignin model compounds [48,49]. Particularly, it was found that the incorporation of Y zeolites promotes the cleavage of intransigent C–C linkages. This interaction effect of NiMo sulfides and Y zeolites was also found to vary with the textural properties, acidity, and dispersion of the active phases [49]. The optimum cleavage of C-O-C and C–C in model dimers was found with NiMoS-USY having a suitable balance of acidic and deoxygenation sites. In addition such proximity effects have also been evaluated using NiMo/HY, $NiMo/Al_2O_3$, and $NiMo/Al_2O_3$ + HY for cyclohexene hydroconversion [50]. The authors claim that the proximity between these sites can enhance the hydrogenation reactions of isomerized products formed on the acidic sites. Sulfided NiMo over pristine Y zeolite (silica/alumina = 2) was also found to be highly active for conversion of orthohydroxy-diphenylmethane to toluene, phenol, benzene and cyclohexane at 235 °C, 155 bar of H_2, and WHSV = 0.49 h^{-1} using a flow microreactor [51].

However, to the best of our knowledge, there are no available investigations regarding the combination of NiMo sulfides with USY zeolites for hydrotreatment of Kraft lignin, which is the objective of the current work. The focus of this study is to gain further insight into the upgradation of a more complex feedstock, Kraft lignin involving NiMo sulfides over ultra-stable Y zeolites. Particularly, the roles of NiMo sulfides and USY zeolites, and their interactions have been explored regarding the depolymerization, HDO, and repolymerization of the reactive intermediates forming solid residues. This study was enabled by screening experiments with NiMo sulfides and various Y zeolites. In addition, control experiments have been made with synthesized unsupported NiMo sulfides as well as experiments in which the catalyst components are combined with different levels of contact. Detailed analysis/characterization of the catalyst has been performed via X-ray diffraction (XRD), H_2-temperature-programmed reduction (TPR), NH_3/$C_2H_5NH_2$-temperature-programmed desorption (TPD), High resolution transmission electron microscope (HRTEM), X-ray photoelectron spectroscopy (XPS), Fourier transformed infrared (FTIR) spectroscopy, ^{13}C nuclear magnetic resonance (NMR) analysis to clarify their roles on the progression of the depolymerization process, resultant product selectivity, and solid residues.

2. Experimental

2.1. Catalyst synthesis

Commercial ultra-stable zeolites, USY (Zeolyst international, molar SiO_2/Al_2O_3 = 30, and 80, hereafter referred to as Y30 and Y80) were calcined in air at 550 °C for 6 h before use. Y80 was dealuminated using 3 M oxalic acid (98%, Aldrich) at 70 °C, stirring at 500 rpm [52]. The time of oxalic acid treatment was varied (16 h and 95 h) to obtain Y zeolites with different levels of dealumination (hereafter termed as Y150 and Y200). Thereafter, the sample was thoroughly washed with Milli-Q water to neutralize the pH. It was then oven-dried (80 °C, overnight), and calcined at 550 °C for 6 h. The pristine Y80 zeolite was also desilicated using 0.2 M (NaOH + tetrapropylammonium bromide, TPABr (PDA)) (98%, Sigma-Aldrich) at 25 °C for 0.5 h. Afterward, the sample was washed to neutralize the pH, oven-dried and calcined. The desilicated sample was further exchanged with 0.5 M NH_4NO_3 at 60 °C for 1 h in three consecutive cycles of ion exchange and centrifugation. The final sample after extensive water washing was dried at 80 °C overnight and

calcined at 550 °C for 6 h.

Ni and Mo were loaded onto commercial and dealuminated/desilicated USY-zeolite samples using a wet impregnation method. The required amount of ammonium molybdate tetrahydrate (99%, Sigma-Aldrich) and nickel (II) nitrate hexahydrate (99%, Sigma-Aldrich) was first dissolved in water and then added dropwise to the zeolite. The mixture was then stirred for 0.5 h at 25 °C. Water was removed via rotary evaporation (85 °C). The resultant mixture was then oven-dried and calcined in air at 450 °C (5 °C/min) for 4 h. The resulting catalysts are abbreviated as NiMo(D)YXX where NiMo stands for Ni and Mo, D for desilication when used, Y for ultra-stable Y zeolite, and XX for the silica-alumina ratio.

Unsupported NiMoS (UNiMoS) catalyst was synthesized hydrothermally largely following a method reported by Wang et. al [20] with some alteration of the synthesis steps. In a typical synthesis, ammonium molybdate tetrahydrate (1.15 g), nickel (II) nitrate hexahydrate, and thiourea (>99 %, Sigma-Aldrich) (4.25 g) were thoroughly dissolved in 180 ml Milli-Q water via stirring. The Ni/Mo mole ratio was kept at 0.5. The pH of the solution was then adjusted to 0.8 using HCl (35 wt%). The mixture was then transferred to a 300 ml Teflon-liner which was then placed in a stainless-steel autoclave reactor. The autoclave was heated in an oven at 200 °C for 12 h. The resulting catalyst was then filtered and washed thoroughly with absolute ethanol before drying under a vacuum in an oven at 50 °C overnight. The catalyst was then characterized and tested without any further pretreatment.

2.2. Catalytic activity measurements

The as-synthesized NiMoY catalysts (0.75 g) were sulfided in an autoclave reactor (300 ml, Parr Inc.) at 340 °C and 40 bar of H_2 (99.9%, AGA) using 0.75 ml DMDS (dimethyl disulfide, ≥99.5%, Sigma-Aldrich). Pre-calcined USY (Y30, Y80) and unsupported UNiMoS were used in the reactor without the pre-sulfidation step mentioned above. 2.25 g of Kraft lignin (Sigma-Aldrich) and 75 ml Hexadecane (99%, Sigma-Aldrich) were added subsequently to the reactor. The reactor was then purged with N_2 and H_2 repeatedly and pressurized to 35 bar at 25 °C. After that, the reactor was heated up to 400 °C with a stirring rate of 1000 rpm which took approximately 45 min. Following heating, the final pressure reached a value of 72–80 bar. The hydrotreatment was then continued for 5 h with a stirring rate of 1000 rpm and then the reactor was cooled down to room temperature with a lower stirring rate (200 rpm). The cooling steps took approximately 25 min. After cooling, the gas sample was collected in a 0.1 L stainless steel cylinder. The reactor was finally purged with N_2 before collecting the liquid and residual solids. The liquid product rich in hexadecane was recovered via vacuum filtration. The lignin derived residue, the emptied reactor vessel, and catalyst samples were then thoroughly washed with acetone, and this resulting liquid product will from here on be referred to as the 'aqueous phase' rich in acetone. The dried lignin solid residue was further washed with dimethyl sulfoxide (≥ 99.9%, VWR) and subsequently with acetone to quantify the unconverted lignin. The complete workup procedure is shown in Figure S1, Supplementary Information (SI). Finally, the solids that remained were dried and further characterized.

2.3. Product analysis

The liquid product samples rich in hexadecane and acetone were analyzed via GC × GC–MS-FID (Agilent 7890B–5977A, Agilent). A mid-polar column (VF-1701MS, 30 m × 250 μm × 0.25 μm) and a non-polar DB-5MS (1.2 m × 150 μm × 0.15 μm) column were used for the separation. The sample was injected via an automatic liquid sampler to the GC injector at 280 °C. The oven temperature was initially kept at 40 °C for 1 min and then ramped to 280 °C with a rate of 2 °C/min. The thermal modulation was kept at 8 s for all the samples. The flame ionization detector was maintained at 250 °C. The 2D chromatograms (MS/FID) thus obtained were thoroughly analyzed via GC Image software. The quantification of the identified monomers, dimers, and polyaromatics are based on external calibrations for each component performed using pyridine as an internal standard. The following equations were used to calculate the Kraft lignin conversion, yields, selectivity for products, and solid residue respectively.

$$Conversion,\ X\ (\%) = \left(1 - \frac{amount\ of\ unconverted\ lignin}{Initial\ dried\ lignin\ charged}\right) \times 100$$

$$Unconverted\ lignin\ (g) = (Dry\ wt.\ of\ acetone\ washed\ solid\ residue - Dry\ wt.\ of\ DMSO\ and\ acetone\ washed\ solid\ residue)$$

$$Yield\ (wt\%) = \frac{amount\ of\ product\ (g)\ after\ 5h}{Initial\ dried\ lignin\ charged\ (g)} \times 100$$

$$Selectivity\ (wt\%) = \frac{amount\ of\ product\ (g)\ after\ 5h}{Total\ detected\ products\ (g)} \times 100$$

$$Solid\ residue\ yield\ (wt\%) = \frac{Dried\ total\ solid\ residue - amount\ of\ catalyst\ charged}{Initial\ dried\ lignin\ charged} \times 100$$

The gas sample was analyzed by a gas chromatograph (SCION 456, Bruker) equipped with both thermal conductivity (TCD) and flame ionization detectors (FID). Quantification of the gas sample was based on external calibrations of CO, CO_2, and C_1-C_5 alkanes/alkenes. The water content in the liquid products was determined by Karl fisher volumetric titration using a Metrohm 870 KF Titrino plus apparatus. About 0.1 ~ 0.2 mg of the sample was titrated with Karl Fischer titrant (HYDRANAL™ - Composite 5, Honeywell Fluka™) in a glass chamber containing HYDRANAL™ - Methanol dry (Honeywell Fluka™).

2.4. Catalyst characterization

N_2 physisorption data were collected using a TriStar 3000 analyzer at −196 °C. The parent and impregnated zeolite samples were dried under nitrogen flow overnight at 220 °C before the measurement. The specific surface area, pore volume, and mesopore sizes were measured using the BET (Brunauer–Emmett–Teller) and BJH (Barrett-Joyner-Halenda)

method. Inductively Coupled Plasma-Sector Field Mass Spectroscopy (ICP-SFMS, ALS Scandinavia AB, Luleå, Sweden) was performed to measure the metal loadings (Ni, Mo), and Si/Al molar ratio of the synthesized catalysts. Temperature programmed-desorption of ethylamine ($C_2H_5NH_2$) and ammonia (NH_3) were performed to measure the acidities of the impregnated catalysts following a method as described in our earlier work [48]. XRD (X-ray diffraction) diffractograms were obtained via a Bruker AXSD8 Advance diffractometer operating at 40 kV and 40 mA with CuKα monochromatic radiation (λ = 1.542 Å) operating with a step size of 0.03° per second. X-ray Photoelectron Spectroscopy (XPS) on sulfided catalysts was performed via Perkin Elmer PHI 5000 VersaProbe III Scanning XPS Microprobes. The sample was irradiated with a monochromatic Al-Kα source (1486.6 eV) in an ultra-high vacuum chamber. Ni2P, Mo3d, C1s, S2p, and O1s core level spectra were recorded with a step size of 0.1 eV to analyze the oxidation state. Deconvolution and fitting of the peaks were performed via CasaXPS using the C1s binding energy of 284.6 eV. The scanning transmission electron microscopy (STEM) images of the sulfided catalysts were recorded via an FEI Titan 80–300 TEM operated at 300 kV using a high angle annular dark field (HAADF) detector and analyzed via TEM Imaging and analysis (TIA) software and ImageJ software. The statistics for estimation of the MoS_2 crystallite dispersion were evaluated in terms of their slab length and stacking as described elsewhere [53].

2.5. Lignin and solid residue characterization

Kraft lignin and catalyst containing solid residue samples were analyzed using Fourier transform infrared spectroscopy (FTIR, Bruker Vertex70v spectrometer) at room temperature. The spectra were recorded in the range of 400–4000 cm^{-1} in a transmittance mode with a resolution of 4 cm^{-1} and 64 scans per sample. Solid-state cross-polarization (CP) ^{13}C NMR spectra were recorded for Kraft lignin and solid residue using a 4 mm MAS BB/^{1}H probe and a Bruker Advance III 500 MHz spectrometer. The rotor was spun at 10 kHz and the CP time was set to 1.5 ms. Thermogravimetric analysis (TGA) of recovered catalyst and Kraft lignin were performed using a Mettler Toledo TGA/DSC 3 + instrument in air and Ar atmospheres respectively.

3. Results and discussion

3.1. Hydrotreatment using impregnated NiMoS over ultra-stable Y zeolites

Fig. 1 summarizes the liquid-phase product and the solid residue yields obtained after the thermal and catalytic hydrotreatments of Kraft lignin at 35 bar of H_2 (@25 °C), 400 °C for 5 h. The overall mass balance was in the range of 73–88 wt% for all experiments (Table S1) based on the initial lignin feed and the measured water produced and products in liquid and gas phases. The discrepancy is due to a minor loss of volatile products from the reactor headspace via condensation while cooling and GC undetectable oligomer products in the liquid phase. In the absence of catalyst, the thermal treatment in H_2 depolymerizes the Kraft lignin. The conversion of lignin was found high (~99%) whereas the yield of the GC detectable monomeric fraction in the liquid product was low (~18 wt %). This is due to the high yield of lignin derived solid residue (~47 wt %) which formed via re-polymerization/ coupling/ condensation reactions of the depolymerized fragments. Preventing these rapid reactions is crucial in the one-pot upgradation process to alleviate the residual solid formation, avoid catalyst deactivation, and obtain a higher yield of monomeric fractions. Kraft Lignin begins to degrade in the temperature range as low as 200–220 °C [12]. As a result, these thermal degradation and repolymerization reactions will start early during the heating process, unless there is a means for fragment stabilization. An active catalyst can stabilize the fragments from thermal depolymerization via hydrogenation of the reactive free radicals, aldehydes, and deoxygenation. Therefore, the catalysts need to be highly active either at such a low temperature or be able to cleave the recalcitrant repolymerized/condensed fractions.

From Fig. 1, depolymerization of Kraft lignin increases in the presence of Y zeolites and sulfided NiMo. Among Y zeolites, Y30 shows a higher yield in the liquid product and less solid residue which indicates that more acidic support is beneficial in cleavage, dehydration, isomerization, and hydrocracking reactions. These Y zeolites impregnated with NiMo sulfides show enhancement of the hydroconversion reactions with a higher yield of the monomeric fraction in the liquid product and lower solid residue (~24%) compared to the bare zeolites. NiMo sulfides over dealuminated supports with increasing silica/alumina ratios of Y150 and Y200 show a clear drop in the depolymerization and a slight

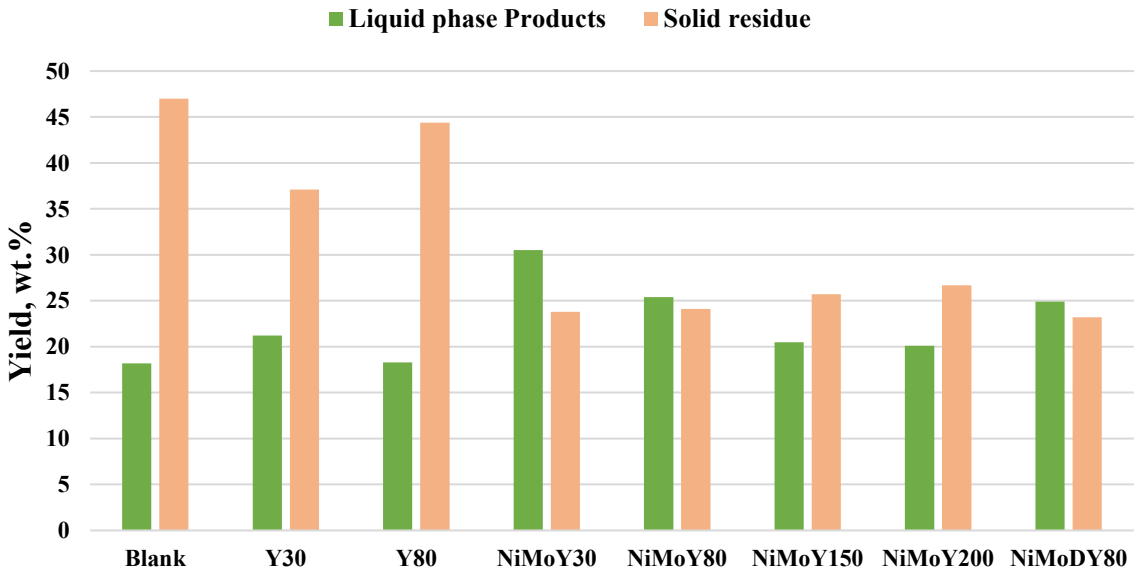

Fig. 1. The yield of liquid-phase products and solid residue during the hydrotreatment of Kraft lignin over sulfided NiMo, Y zeolites and in absence of catalyst (blank) at 400 °C, 35 bar H_2 (@25 °C), and 1000 rpm for 5 h.

Table 1
Yield and selectivity of products from the hydrotreatment of Kraft lignin over sulfided NiMo and USY zeolite at 400 °C, 35 bar H_2 (@25 °C), and 1000 rpm for 5 h.

Catalyst	Liquid Yield. (wt. %)	Liquid product selectivity (%)					Solid residue. (wt. %)
		Cycloalkanes/ Alkylbenzenes	Phenols	Indans/Napthalenes/ Biphenyls	Polycyclic aromatics	Other oxygenates	
Blank	18.2	10	60	5	13	13	47
Y80	18.3	10	60	5	13	13	44.4
Y30	21.2	29	47	10	10	4	37.1
NiMoY30	30.5	61	1	27	9	2	23.8
UNiMoS	23.5	42	25	8	24	2	25.2
UNiMoS + Y30	29.1	30	27	20	21	2	16.7
NiMoY30*	38.9	79	0	14.5	4.9	1.5	16.4
NiMoY80	25.4	49	2	26	21	2	24.1
NiMoY150	20.5	58	7.5	18	13.5	3	25.7
NiMoY200	20.1	59	7	16	16	2	26.7
NiMoDY80	24.9	46	11	21	19	3	23.2

*Extending residence time to 8 h and decreasing lignin catalyst ratio from 3:1 to 2:1.

increase in the solid residue formation. Among the above results, NiMoY30 shows a notable liquid product yield (30.5%). However, the higher yield of solid residue (~24%) at the end of the 5 h reaction implies that significant re-polymerization of the lignin fragments has occurred. This could be due to diffusion limitations for the bulkier lignin fragments to enter the zeolite pores and access the active sites or the active site inhibition by the lignin impurities (e.g., alkali metals). To understand the influence of the diffusion limitations, Y80 was desilicated (*see Section 2.1*) and impregnated with NiMo. The result shows little variation in the liquid and solid residue yields compared to NiMoY80. This led us to synthesize an unsupported NiMoS catalyst to obtain mechanistic insights into lignin hydrotreatment with this catalytic system.

3.2. Role of NiMoS and Y30 in Kraft lignin hydrotreatment

To elucidate the role and interactions of the catalyst components (NiMoY30), control experiments have been performed using unsupported UNiMoS and Y30. It is important to note that the amount of UNiMoS is chosen to match the nominal loading of Ni and Mo in NiMoY30, i.e., the reactor is loaded with equal masses of transition metals in all experiments. As seen from Table 1, for the equivalent amount of UNiMoS alone as in the impregnated catalyst, the GC–MS detectable liquid product yield was lower than for NiMoY30 while for the physical mixture of UNiMoS and Y30, the yield is comparable to that for NiMoY30.

Similarly, for UNiMoS the solid residue was ~ 25 wt% and just slightly higher than for NiMoY30, while for the physical mixture, interestingly the solid residue decreased to 16.7 wt%. These experimental results further demonstrate that Y30 has a positive role in lignin fragment stabilization. It also gives an insight into the one-pot lignin valorization using NiMoS catalyst.

Typically, the thermal decomposition of lignin results in the formation of free radicals (phenoxyl, methoxy, methyl, etc.) [54]. Stabilization of these free radical fragments is crucial to prevent coupling/recombination reactions and solid residue formation. The presence of H_2 and capping agents (e.g., phenol, boric acid, etc.) has been reported to be beneficial to stabilize them and obtain higher yields of depolymerization products [55,56]. The reaction of H_2 with these radicals thus plays an important role. Impregnated NiMoS and UNiMoS in this regard are vital as they facilitate hydrogen dissociation at the reaction conditions to form metal-SH and metal-H species and sulfur vacancies on the catalytic surfaces [57–60]. As a result, dissociated surface hydrogen can be transferred to the adsorbed radicals for the stabilization process. Also, the availability of the active sites of NiMoS for the radicals/fragments is also important. Since NiMoY30 yielded a higher solid residue compared to the physical mixture of UNiMoS + Y30 it can be inferred that the Ni-promoted MoS_2 sites were less accessible to the large lignin radicals especially those that are deep inside the Y zeolite channels/pores, while unsupported UNiMoS sites are more readily accessible. In addition, Y-zeolite can also stabilize the fragments via proton donation. This enables the stabilization of more lignin fragments, and it results in lower solid

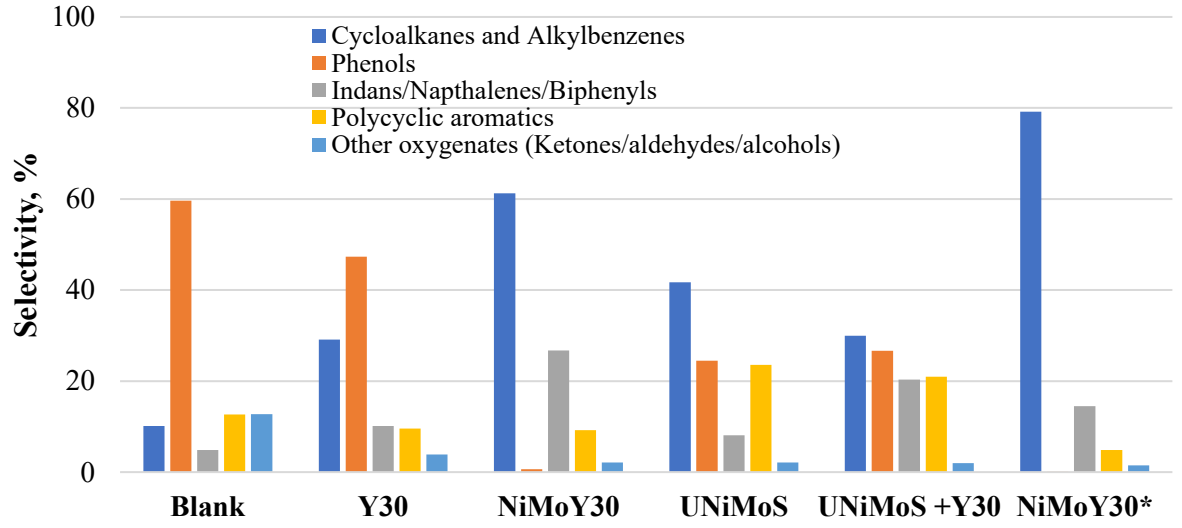

Fig. 2. Liquid product selectivity for the hydrotreatment of Kraft lignin in absence of catalyst (Blank) and over NiMo and Y-zeolite catalysts at 400 °C, 35 bar of H_2 (@25 °C), and 1000 rpm.

residue for the physical mixture compared to the UNiMoS. However, for the impregnated catalyst (NiMoY30), higher liquid yield compared to other impregnated catalysts listed in Table 1 could be attributed to the better surface proximity of the Ni-promoted MoS_2 sites and acidic sites. From Table 1, it is clear that Y30 has a positive influence on lignin depolymerization, stabilization reactions both alone compared to the blank experiment and when combined with unsupported UNiMoS. It also contributes to hydrocracking reactions. The extent of the hydrocracking reaction seems higher when it is impregnated with NiMo. There is a small variation in the gas phase products and water content from these experiments (Table S1). It is noteworthy to mention that unsupported UNiMoS and the physical mixture were examined/compared here solely to clarify the role of impregnated NiMoS and Y30. Differences in their properties may also contribute to varying product yields which will further be discussed in detail in *Section 3.3*.

Table 1 and Fig. 2 compare the liquid product selectivity based on the quantification of the identified products from 2D GC × GC–MS images (Figure S2a, Table S2). For simplicity, products were grouped into cycloalkanes (or naphthenes), alkylbenzenes, phenols, indans, naphthalenes, biphenyls, polycyclic aromatics, and other oxygenates. Other oxygenates mainly include aldehydes, ketones, and alcohols. Under the H_2 environment, phenols (mainly alkylphenols) are the dominant fraction of products from the blank and Y30 experiments without NiMo.

Y30 also shows up to ~ 29% yield of alkylbenzenes (traces of cycloalkanes) showing its demethoxylation, dehydration, and deoxygenation activity, albeit to a lesser extent. With the NiMo impregnation of Y30, the foremost fraction becomes the cycloalkanes and alkylbenzenes for all the studied catalysts. Interestingly, NiMoY30 (lignin to catalyst mass ratio of 3) showed a high selectivity (~61%) for monocyclics and alkylbenzenes. Among these products, monocyclics contributed to ~ 24% and alkylbenzenes to ~ 37%. Y80-zeolite and its dealuminated variants impregnated with NiMo (Table 1) showed a similar trend but with lower yields of cycloalkanes and alkylbenzenes than NiMoY30. The lower yield of polycyclic fractions in NiMoY150/NiMoY200 than NiMoY80 (Table 1) indicates a higher extent of hydrocracking due to their enhanced access and lower diffusion resistance to reach active sites, resulting in an improved monomer selectivity. The high amount of alkylbenzenes with NiMo-based Y zeolites demonstrates the preference for the direct-deoxygenation reaction route over the ring-hydrogenation route for the depolymerized/stabilized oxygenate fragments during the hydrotreatment at 400 °C. A high amount of cycloparaffins and alkylbenzenes are suitable for jet fuel applications [61].

Notably, the physical mixture of UNiMoS and Y30 had a lower selectivity for these deoxygenated products while the selectivity for phenols increased to 27% compared to 1% for the impregnated NiMoY30. The phenol selectivity was also high with UNiMoS (~25%) indicating its ability to stabilize the lignin fragments and hinder the formation of solid residues. The significant monocyclics and alkylbenzenes yield with NiMoY30 can also be due to the presence of a low amount of polycyclic aromatics (Table 1). These polycyclic mainly form by deoxygenation reactions catalyzed by NiMo. They can also be formed via linear or angular fusion of the monomeric benzene/aromatic rings. With NiMoY30, the selectivity for this group amounted to $< 10\%$ while for the other NiMo-based catalysts (except dealuminated and desilicated USY samples) it is $\geq 20\%$. This implies that having Y30 and its acid sites in closer contact with NiMo prevents the formation of such polycyclics to a greater extent. Also, when formed, hydrocracking reactions can occur to some extent due to the presence of Brønsted acidic sites [62]. The physical mixture of UNiMoS and Y30 (UNiMoS + Y30) resulted in only a slight reduction in polycyclics compared to UNiMoS alone. This underlines the importance of a close contact between deoxygenation and acid sites to prevent polycyclic formation. It is hindered in Y30 partly also due to the limited diffusion of polycyclics in the zeolite and thus greater chance that they undergo hydrocracking reactions. An extended 8 h reaction (from 5 h) with lower lignin to catalyst (NiMoY30) mass ratio of 2:1 (from 3:1) showed significant enhancement in the depolymerization, deoxygenation, isomerization, and hydrocracking reactions leading to a lower solid residue (Table 1). As a result, the liquid product yield increased to 38.9 wt% with a remarkable alkylbenzene selectivity of ~ 72%, making a total of 79% selectivity for both monocyclics and alkylbenzenes. This is a remarkable monomer product yield compared to reported literature results for lignin valorization over sulfided NiMo based catalysts (Table S3). In addition, the formation of polycyclics was further reduced to a value of 4.9% selectivity.

With the desilicated NiMoDY80, it is evident that phenol selectivity increased to 11% compared to 2 % for NiMoY80 giving rise to a small increase in overall monomer (cycloalkane, alkylbenzene, and phenol) selectivity (57% vs 51% for NiMoY80). The selectivities for other products are somewhat lower than for the NiMoY80. The yield of solid residue is slightly lower than NiMoY80. This result demonstrates that desilication had little influence on the Kraft lignin depolymerization and further processing.

To understand more about the solid residue formation, an additional experiment was performed with pre-sulfided NiMoY30, where the reaction was stopped by rapidly cooling the reactor (taking approximately 25 min) once the target temperature of 400 °C was reached. The result shows that the yield of liquid-phase products was only ~ 13.4 wt% (Table S1) with an alkylphenol selectivity of 52% (not shown) whereas a major fraction of the lignin ends up as solid residue (~34.5 wt%) even in the presence of catalysts. The fact that this solid residue yield is comparable to that with the same catalyst and 5 h reaction time at 400 °C (30.5 wt%) indicates that the depolymerization and fragment coupling reactions already begin at lower temperatures during reactor heating, during which a large part of the solid residue is formed. Furthermore, 5 h reactions with sulfided NiMoY30 at a lower temperature of 340° C and 250° C showed substantially increased solid residue yields of 35 wt% (99% conversion of lignin) and 67 wt% (94% conversion of lignin) respectively demonstrating the extent to which the fragment coupling/condensation reactions dominate over catalytic reactions stabilizing the depolymerized fragments at lower temperatures. The synthesized catalysts are characterized in detail to shed light on their behavior in the subsequent sections.

3.3. Characterization of the catalysts

3.3.1. Textual properties and metal contents of the synthesized catalysts

The composition and textural properties of the synthesized catalysts are listed in Table 2. It can be seen that oxalic acid treatment removes framework aluminum efficiently, which results in a higher silica/alumina ratio in the desired range as listed for Y150 and Y200 (Table 2). With these dealuminated Y-zeolites, the external surface area and mesopore size/volume increase while the total specific BET area decreases slightly. Desilicated Y80 (DY80) shows a high external surface, accounting for 53% of the total BET surface area, mainly due to the creation of mesopores at the expense of micropores in the parent Y80. The physisorption isotherms for the parent and desilicated zeolites are shown in Figure S3a. This increment in the pore sizes (via dealumination and desilication), could allow better access for depolymerized lignin fragments to reach the NiMo sites in the zeolite. Impregnating these zeolites with NiMo physically blocks the pores and reduces both total and external surface areas, as well as pore sizes as shown in Table 2. According to ICP-SFMS, the overall obtained Mo and Ni loadings were in the range of 12–13 wt% and 3.7–4.5 wt% respectively for all the supported catalysts. Figure S3b compares the isothermal nitrogen adsorption/desorption data and BJH pore size distributions for the as-synthesized NiMoY30 and UNiMoS. As can be seen, hydrothermal synthesis of UNiMoS gives a BET surface area of 49 m^2/g with an average pore diameter of 11.5 nm. The NiMoY30 has a high external surface area (126 m^2/g), with mesopores in the range of 2–4 nm. The atomic ratio of Ni/(Ni + Mo) for the supported catalysts was in the range of 0.33–0.37 and for unsupported UNiMoS, it was 0.31.

Table 2
Composition and textural properties of the synthesized and sulfided catalysts.

Catalyst	Elemental composition (wt. %)				N_2 physisorption			
					$S_{a.\ total}$	$S_{a.\ external}$	$V_{p.total}$ ($V_{p.meso}$)	d_p
	SiO_2/Al_2O_3[b]	Mo	Ni	Atomic ratio Ni/(Ni + Mo)	(m^2/g)	(m^2/g)	(cm^3/g)	(Å)
Y30	25	–	–	–	801	234	0.54 (0.26)	40.9
NiMoY30	–	12.7	4.5	0.37	514	126	0.33 (0.14)	44.3
Y80	88	–	–	–	808	243	0.56 (0.29)	39.3
NiMoY80	–	13.0	4.4	0.36	500	165	0.33 (0.17)	37.8
Y150	146	–	–	–	792	279	0.57 (0.32)	41.3
NiMoY150	–	12.8	4.4	0.36	398	175	0.33 (0.20)	41.6
Y200	212	–	–	–	737	268	0.57 (0.34)	43.8
NiMoY200	–	12.6	4.4	0.36	423	148	0.32 (0.19)	43.8
DY80	69	–	–	–	662	353	0.68 (0.53)	49.3
NiMoDY80	–	12.4	3.7	0.33	344	213	0.40 (0.34)	50.3
UNiMoS	–	29.8	8.4	0.31	49	49	0.22	115.2

* S_a = BET surface area. V_p = Pore volume. d_p = Average pore sizes for mesopores. b = measured by ICP-SFMS.

Table 3
Total acidity and Brønsted acidity of the synthesized catalysts measured by NH_3 and ethylamine temperature-programmed desorption.

Catalyst	Total acidity (NH_3-TPD)	Brønsted acidity ($C_2H_5NH_2$-TPD)	Lewis acidity*
	(μmol g^{-1})	(μmol g^{-1})	(μmol g^{-1})
Y30	478	386	92
NiMoY30	608	300	308
Y80	248	221	27
NiMoY80	424	217	207
NiMoY150	397	123	274
NiMoY200	348	102	248
NiMoYDY80	515	222	293
UNiMoS	158	–	–

*Estimated from the difference between total and Brønsted acidity.

3.3.2. *NH_3 and $C_2H_5NH_2$ temperature-program desorption (TPD) analysis*

The acidity of the catalyst was determined via NH_3 (NH_3-TPD) and ethylamine ($C_2H_5NH_2$-TPD) temperature-programmed desorption. The results are shown in Table 3, with the corresponding desorption profiles in Fig. 3. The total acidity of the parent Y-zeolites is lower, and a major fraction is due to Brønsted acidity. Impregnating these zeolites with NiMo causes a significant augmentation in the total acidity, presumably due to the formation of new Lewis acidic sites. A decrement in the Brønsted acid sites after metal impregnation (NiMoY30/ NiMoY80) is either due to pore blockage or possible exchange of metal ions during impregnation. The total acidity of the NiMo impregnated and desilicated Y80 is between that of NiMoY30 and NiMoY80, however, the Bronsted acidity is mostly retained from the parent Y80. The difference in acidity plays a vital role in the lignin depolymerization and upgradation *(vide supra)*.

Deconvolution of the NH_3-desorption peak (Figure S4, Table S4) demonstrates that the total acidity is comprised of sites with varying acid strength. As noticed, the acidity fraction corresponding to NH_3-desorption ≥ 250 °C decreases with the increasing silica/alumina ratio (see Figure S4, Table S4). This indicates that with a higher silica/alumina ratio, catalysts not only have fewer total acidic sites but also lose more of the strongest acidic sites. It is thus both the higher number and strength of acidic sites in the resulting catalyst that affects the depolymerization and the further upgradation. From the reactivity data (Table 1, Figure S2a), these acidic sites contribute to the hydrogenolysis, isomerization/transalkylation, hydrocracking, and dehydration reactions as evident from the product spectrum in Fig. 2.

The yield of the liquid product also correlates well with the overall and Brønsted acidities of the catalyst as shown in Fig. 4a. Though Lewis acidity does not correlate to the liquid product yield (Fig. 4a), it plays a major role in hydrogenolysis, deoxygenation and hydrogenation reactions. This can be deduced by comparing the experimental results of Y30/Y80 which are mostly composed of Brønsted acidic sites (Table 3). A higher concentration of Brønsted acidic sites in Y30 than Y80 increases the lignin depolymerization and reduces the solid residue formation (Fig. 1). As observed earlier, the product spectrum shows a relatively

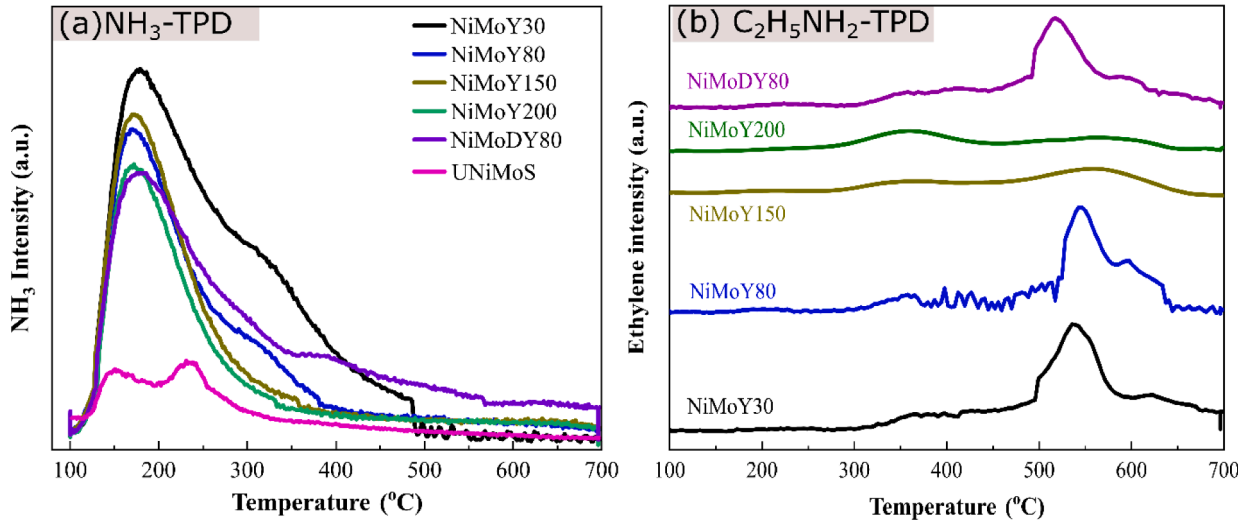

Fig. 3. Desorption profiles for (a) NH_3 and (b) ethylamine temperature-programmed desorption.

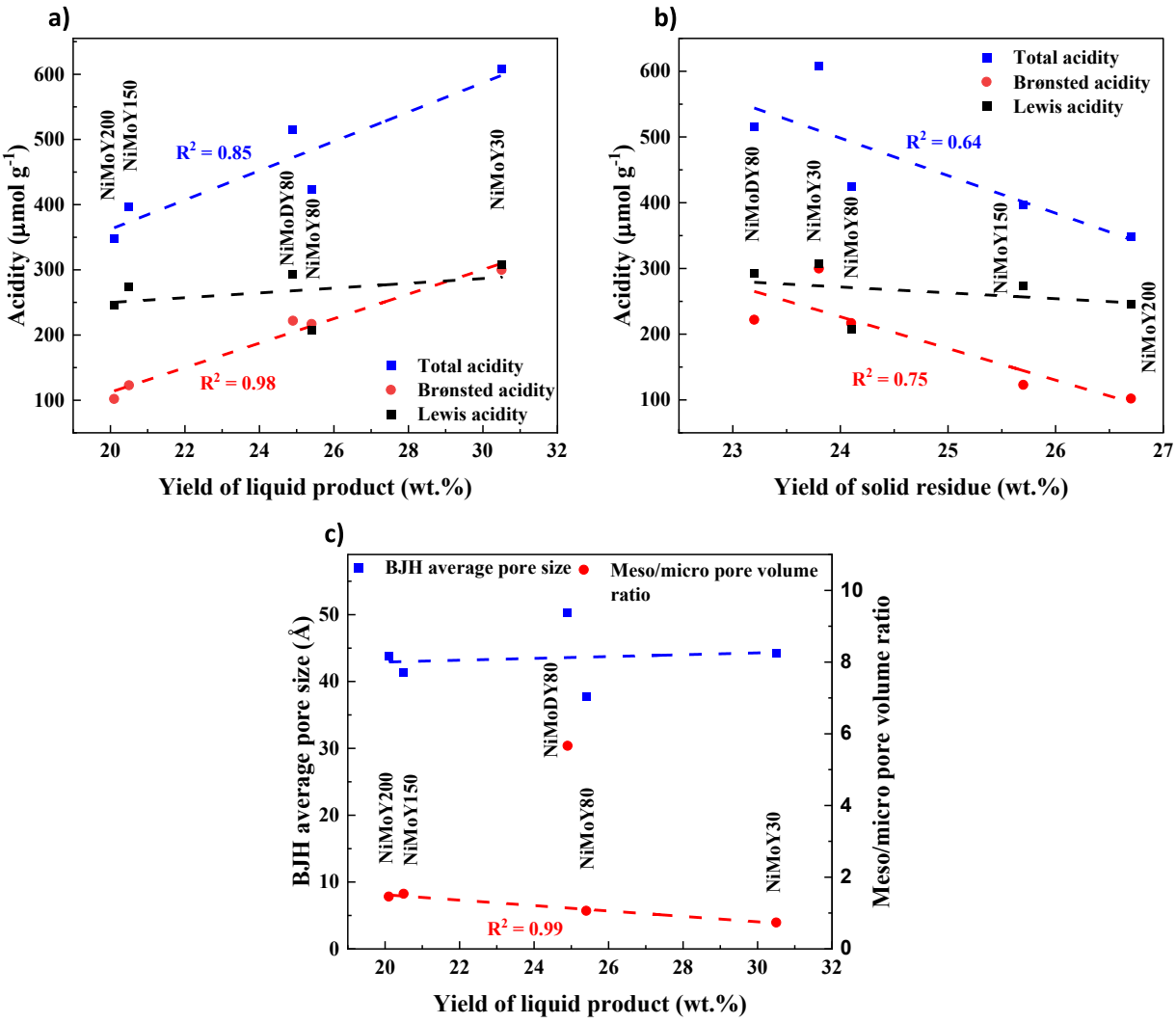

Fig. 4. Correlation of the total and Brønsted acidity of the catalyst to the (a) yield of liquid product and (b) yield of solid residue and (c) correlation of the textural properties of the catalyst to the yield of liquid products after the hydrotreatment of Kraft lignin over NiMo impregnated Y zeolites. Dashed lines indicate linear correlations along with their coefficients of determination (R^2-values).

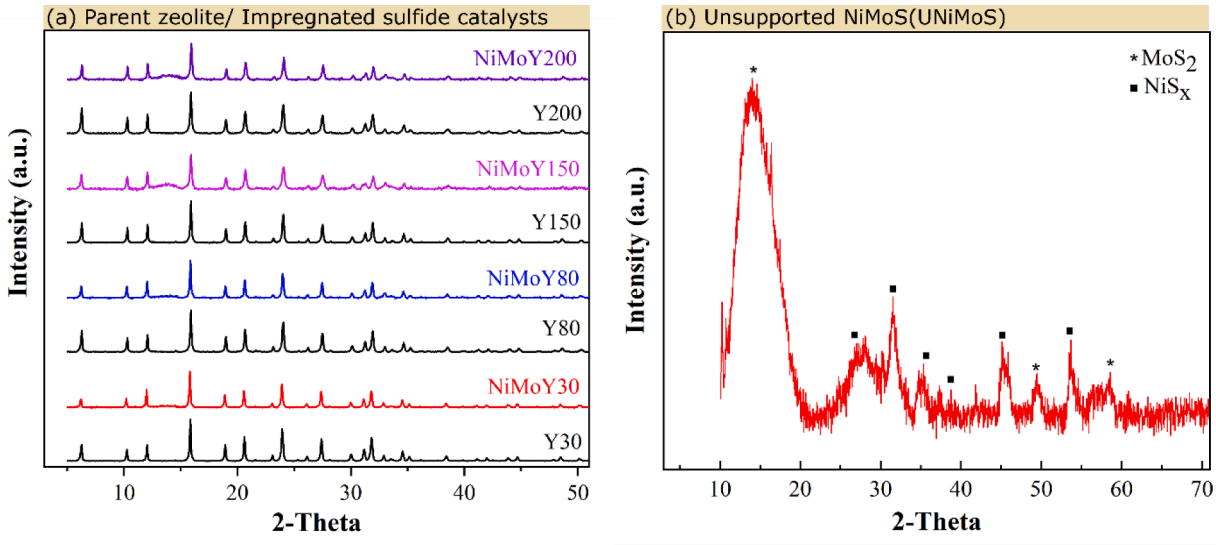

Fig. 5. X-ray diffraction patterns of (a) parent zeolites and zeolites impregnated NiMo sulfides, (b) Unsupported NiMoS (UNiMoS).

higher alkylbenzene, and low polycyclic fraction for Y30/Y80 than the blank experiment (Figure S2b) showing the ability of Y30/Y80 to donate protons to induce C–C cleavage reactions. However, high phenol selectivity over them indicates the lower deoxygenation activity of Y zeolite as consistent with literature [46]. Our earlier work with model compounds shows that the USY support with higher Brønsted site quantities also promote acid catalyzed dehydration, transalkylation and isomerization reactions [11,12]. The increased acidity of NiMoY30/NiMoY80 (due to an increase in Lewis acidity) enhances depolymerization [63] and upgradation via hydrogenolysis, deoxygenation, and hydrogenation reactions leading to a fraction composed mainly of alkylbenzene and monocyclics. High deoxygenation activity (lower phenol selectivity than Y30, Fig. 2) of UNiMoS can be attributed to the presence of sulfur vacancies (coordinatively unsaturated sites, CUS sites act as Lewis acid). However, increased formation of polycyclic compounds over UNiMoS shows the necessity of Brønsted acidic sites for C–C cleavage [6]. Overall, NiMoY30 with optimized Brønsted and Lewis acid sites shows higher depolymerized fractions and high selectivity to cycloalkanes and alkylbenzenes.

On the other hand, lower overall acidity (due to lower Brønsted acid site density) for the dealuminated catalysts results in lower monomer yields with a slight increase in the solid residue (Table 1). The variation in solid residue formation correlates only weakly with the variation in the acidity of the catalysts (Fig. 4b). However, in Table 1, it appears that there is a slightly lower yield of polycyclic products for NiMoY150/NiMoY200 than NiMoY80 which suggests that larger pores may have allowed for more hydrocracking of these larger compounds. Desilicated Y zeolites with NiMo on the other hand, having higher overall acidity and meso/micropore volume ratio than the NiMoY80 demonstrated little influence on the Kraft lignin hydrotreatment. This could be due to the loss of crystallinity of the zeolite framework (Figure S5) or due to variations in the dispersion of the active phase (not investigated here). Fig. 4c indicates there is an excellent correlation between the meso/micro pore volume ratio of the dealuminated USY catalysts (NiMoY30 to NiMoY200) and the yield of the liquid product. However, the desilicated NiMoDY80 clearly deviates from this correlation in Fig. 4c. Although, in Fig. 4a it is evident that the acidity of the NiMoDY80 catalyst correlates well with the liquid product yield along with the dealuminated catalysts.

3.3.3. X-ray diffraction (XRD) analysis

The XRD patterns for the parent, dealuminated and NiMo impregnated USY zeolite after calcination and sulfidation are shown in Fig. 5. Dealumination by oxalic acid causes some crystallinity losses. Based on the peak around 16° for Y80, the relative crystallinity for Y150 and Y200 were found to be 91% and 84% respectively. Also, among the USY zeolites, the peak around 6.3° shows some small variation (5–10 %) compared to the peak around 16° due to loss of crystallinity and changes in the textural properties as evident from the BET data (Table 2). NiMo impregnation causes further amorphization of the USY structure and crystallinity losses mainly due to pore blockage and compressive strain development. As a result, peak intensity reduces further which is consistent with findings in our earlier work [48,49]. The absence of a distinct diffraction peak for Ni and Mo containing crystallites indicates that both phases are dispersed quite well, or they have a low crystallinity, and/or the sulfided phases are amorphous. Indeed, the amorphous nature of as-synthesized unsupported UNiMoS can be seen in Fig. 5(b). The observed diffraction peaks at 2-theta values of 14°, 49.5°, and 59° represent the (002), (105), and (103) characteristic planes respectively of 2H-MoS_2 (Hexagonal MoS_2) [13,64]. However, the peaks at 27.3°, 31.5°, 35.3°, 38.7°, 45.3°, 53,6°, 58.7° indicate the presence of (111), (200), (210), (211), (220) and (311) and (230) planes respectively of NiS_2 [65–68]. The result for UNiMoS is shown in Fig. 5b and the UNiMoS sample consists of Ni sulfide phases in addition to the Ni-promoted MoS_2 phases.

XRD patterns of the desilicated Y80 (DY80) and NiMo impregnated oxide catalysts are shown in the supplementary Figure S5. Consistently,

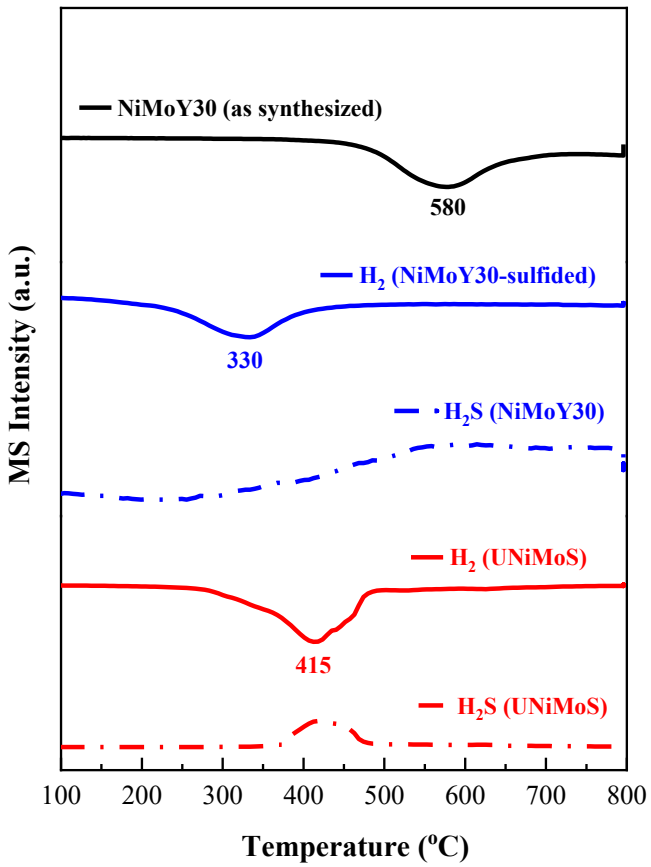

Fig. 6. H_2 uptake characteristics of UNiMoS, sulfided and as-synthesized NiMoY30 during H_2-Temperature programmed reduction.

USY structures are very prone to collapse under alkaline treatment (0.2 M NaOH, Figure S5), however, thanks to tetra propylammonium bromide added as a pore directing agent the crystallinity could be retained to some degree during desilication [69–71]. Although the desilication process creates mesopores (Table 2) and stronger acid sites above 400 °C (comparing Figure S4) it is possibly the moderate acidic sites that most effectively catalyze the lignin depolymerization and isomerization reactions at the studied reaction conditions. NiMoDY80 contains a lower fraction of these sites which could be a reason for its low activity in this study. In addition, the significant micropore loss can affect the framework stability and shape-selective isomerization functionalities [40,72].

3.3.4. H_2-Temperature program reduction (TPR) analysis

H_2-TPR was performed to illustrate the H_2 uptake characteristics of unsupported UNiMoS and the impregnated NiMoY30. The results are shown in Fig. 6. The low-temperature shoulder (for NiMoY30, ~230 °C) indicates either the presence of non-stoichiometric sulfur or weakly bonded sulfur such as -SH groups [73,74]. The high-temperature peak (~330 °C for NiMoY30, ~ 415 °C for UNiMoS) can be related to strongly bound sulfur species. As synthesized NiMoY30 (oxide phases) show a reduced peak at a very high temperature (~580 °C). It is evident that for UNiMoS, H_2 uptake results in the simultaneous release of a small amount of H_2S indicating the creation of so-called sulfur vacancies by weakening the Mo-S bond [59]. H_2S release from sulfided NiMoY30 is delayed compared to UNiMoS and requires a higher temperature to create more sulfur vacancies. This can affect the hydrogenolysis/deoxygenation activities of the two catalysts. Indeed, a higher deoxygenation activity was observed for NiMoY30 than UNiMoS and UNiMoS + Y30 (Table 1). Again, comparing the two H_2 uptake characteristics, UNiMoS starts to consume H_2 at a higher temperature while NiMoY30 at a lower temperature. This discrepancy could arise either from differences in their

structural composition/morphology due to dissimilar synthesis methods or differences in the diffusion characteristics. However, both these temperatures are higher than the Kraft lignin degradation temperature (~200 °C) [12]. This suggests that lignin fragments via depolymerization under the reaction conditions may undergo recombination/radical coupling reactions at lower temperatures than the H_2-activated stabilization by the supported or unsupported NiMo sulfide catalysts. As the temperature increases during the heating of the reactor at start-up, the surface coverage of dissociated hydrogen increases and leads to the formation of sulfur vacancies. Depolymerization via hydrogenolysis, stabilization of fragments, and HDO reactions thus proceed simultaneously where H_2 plays a crucial role in all these steps. It can be seen from the Fig. 6 that NiMoS in the impregnated condition (sulfided NiMoY30) can activate hydrogen at lower temperature than UNiMoS. The other zeolites impregnated with NiMo are expected to have similar characteristics (not shown in Fig. 6).

To illustrate the effect of H_2 uptake and the coupling/recombination reactions, additional experiments were performed with pre-sulfided NiMoY30 catalyst (*discussed in Section 3.2*). Based on these observation it can be deduced that the effective utilization of unsupported UNiMoS or NiMo impregnated catalysts to yield minimal solid residue necessitates an improved lower temperature activity of the catalyst or design of the reactor allowing the lignin to be introduced at the desired temperature where the NiMoS is highly active. An increased amount of accessible catalytic active sites can also play an important role as *discussed in Section 3.2* [12].

3.3.5. X-ray photoelectron spectroscopy (XPS) and transmission electron microscopy (TEM) analysis

XPS analysis revealed that Mo and Ni were mostly present in the form of metal sulfides as indicated by the deconvolution of Mo3d, Ni2p, and S2p core level spectra as shown in Fig. 7. MoS_2 (228.6 ± 0.1 eV) NiS_x (852.8 ± 0.1) and NiMoS (854.2 ±0.2) are the major sulfide phases identified for both the unsupported NiMoS and supported NiMoY30. A small contribution of Mo^{5+} corresponding to oxysulfide was observed for both samples but to a higher extent for unsupported UNiMoS. Unsupported UNiMoS also showed a minor contribution from a metal sulfate peak at a binding energy of 169 eV probably formed during the hydrothermal synthesis. This was absent for NiMoY30. More NiS_x phase was observed for NiMoY30 than UNiMoS. Overall Ni sulfidation was found higher for NiMoY30, i.e., 90% vs 79% (see Table 4). XPS analysis also shows an unexpectedly low amount of surface Ni/(Ni + Mo) atomic ratio for UNiMoS compared to NiMoY30 indicating Ni is mostly present in the bulk.

TEM data of the UNiMoS and NiMoY30 catalysts is shown in Fig. 8. An overview of the materials shows UNiMoS fringes as micelles and the NiMo sulfide particles over Y30 (Fig. 8(I)). STEM-High angle annular dark field (HAADF) and STEM-EDX mapping over a characteristic area on both surfaces show a uniform distribution of elemental Mo, Ni, and S (Fig. 8(II-V). The bright-field (BF) TEM micrograph shows the fringes/layered structure with a characteristic interlayer distance of 0.62 nm corresponding to the (0 0 2) crystal planes of MoS_2 (Fig. 8(VI)). However, careful observation of these HRTEM images shows distinct differences in their developed morphology. More bending and sharper edges of the promoted MoS_2 slabs were evident for UNiMoS leading to the formation of more defect-rich (active) sites for catalytic reactions (Fig. 8a (VI)) [64,75]. This is due to the growth of fine MoS_2 crystallites at the edges giving rise to a porous nature and easy access for the incumbent molecules. NiMoY30 on the other hand had more rounded/curved features (Fig. 8b(VI)) that may result from steric hindrance from the Y30 support.

According to Table 4, it is evident that the UNiMoS sample shows lower MoS_2 dispersion, but more edge Mo sites due to a higher average slab length and lower stacking (Figure S6). On the other hand, supported NiMoY30 shows higher MoS_2 dispersion with a greater amount of corner sites than UNiMoS. This comparison reveals that UNiMoS having more edge Mo atoms (1.6-fold time) should facilitate higher hydrogenolysis reaction activity than NiMoY30 per mass of the metals. Additionally, analysis of the STEM-HAADF and STEM-EDX shows areas lean in Mo while rich in Ni without significant difference in the sulfur distribution on the UNiMoS catalyst (Figure S7). This indicates a greater presence of NiS_x phases and is consistent with the literature [76–78].

The XPS and TEM characterization results indicate that the impregnated and unsupported NiMo sulfides are composed of mixed NiSx and MoS_2 phases. This is in line with XRD measurements (Fig. 5(b)). But a relatively higher fraction of NiS_x over NiMoY30 (Table 4) may induce lower coordination of Ni to edge Mo atoms of the MoS_2 that weaken the Mo-S bond. Li et al [39] stated that the existence of NiS_x clusters can

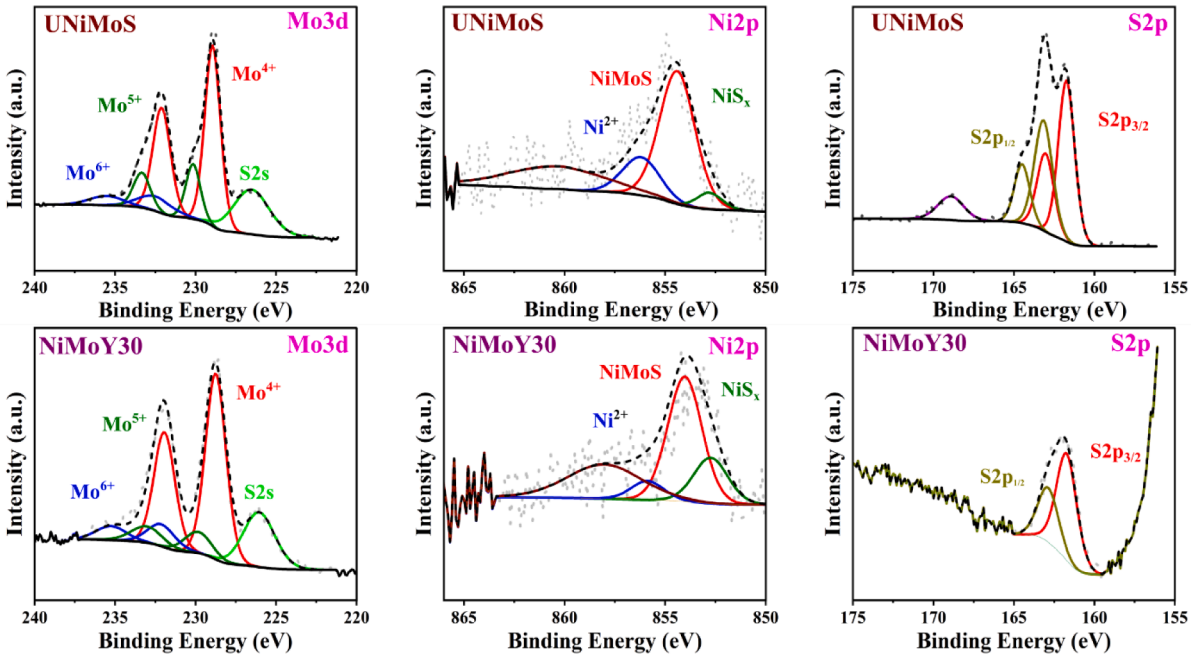

Fig. 7. Core level XPS spectra for Mo3d, Ni2p, S2p of UNiMoS and sulfided NiMoY30 samples.

Table 4
Data from the XPS and TEM analysis of the supported/unsupported sulfided catalysts.

Catalyst	Mo Sulfidation (%)	Ni Sulfidation (%)			Ni/(Ni + Mo) atomic ratio	Average Slab length (nm)	Average Stacking	MoS_2 dispersion, f_{Mo}	Edge to corner ratio
	Mo^{4+}/Mo^{5+}	NiS_x	NiMoS	Ni^{2+}					
UNiMoS	68/20	7	72	21	0.05	6.3	2.9	0.156	8.4
NiMoY30	75/13	24	66	10	0.22	4.3	3.8	0.254	5.2

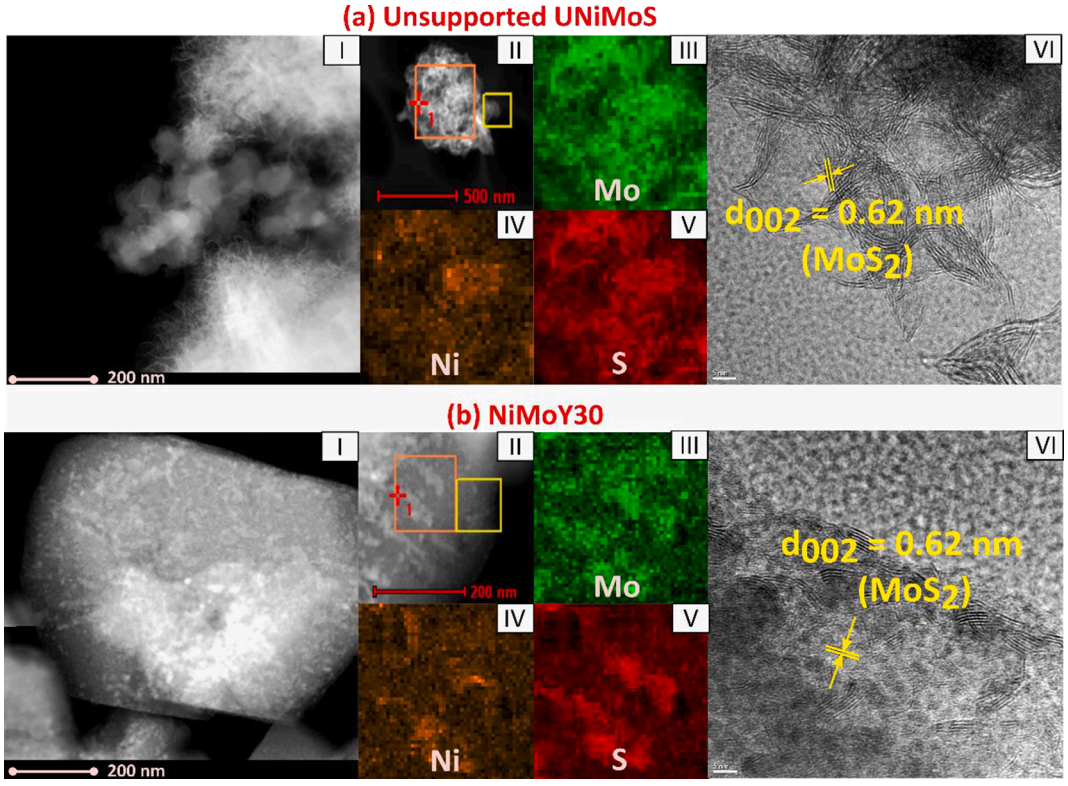

Fig. 8. HAADF-STEM/HRTEM imaging and EDX mapping of (a) Unsupported NiMoS and (b) NiMoY30. Sub images: (I) overview of the materials, (II) overview of the analysis area (orange box), (III) Molybdenum, (IV) Nickel, (V) Sulfur EDX elemental mapping, and (VI) BF-TEM micrograph.

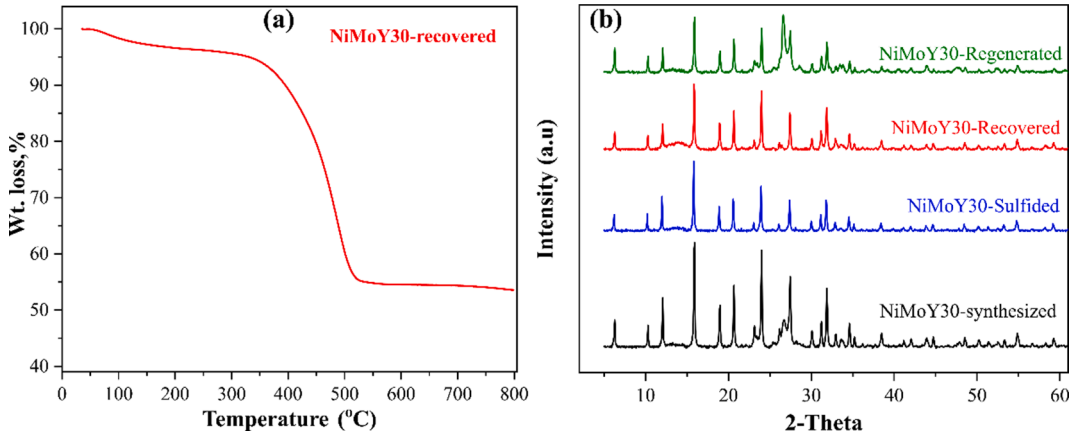

Fig. 9. (a) Thermogravimetric analysis of the solids recovered from reactor following NiMoY30 hydrotreatment and (b) XRD pattern of the NiMoY30 following different stages.

promote the hydrogenation activity of MoS_2. K. Wu et al. [15] suggested that synergetic effects between NiS_2 and MoS_2 enhance the hydrogenation and HDO reaction of 4-ethylphenol and 4-propylguaiacol. Excess NiS_x, on the other hand, can lower the activity by masking the active sites of MoS_2 [76]. However, H_2-TPR results demonstrate that Ni incorporation weakens the Mo-S bond at the edges, as the H_2-uptake temperature shifted to a lower temperature for NiMoY30 compared to UNiMoS, which promotes the formation of sulfur vacancies, metal hydrides and sulfyhydryl groups. Apart from these aspects, the morphology of the resulting sulfided phases also plays an important role in their ultimate reactivity. The observed reactivity for NiMoY30 thus can be attributed to hydrogen activation at a lower temperature, a higher dispersion of Ni promoted MoS_2 leading to a 5-fold abundance of edge Mo atoms rather than corner atoms which are responsible for hydrogenolysis and hydrogenation reactions. In addition, the acidity of NiMoY30 shows the importance of alkylation (isomerization), hydrocracking, and dehydration activities. Nevertheless, the textural properties probably limit the accessibility of the large lignin fragments to exploit the full potential of sulfided NiMoY30, resulting in the formation of more residual solids and deactivation.

3.3.6. Thermogravimetric analysis (TGA) of solid residue and regeneration of NiMoY30

The solid residue generated with NiMoY30 during the catalytic hydrotreatment was analyzed via TGA in the air as shown in Fig. 9 (a). It is important to note here that solid residue recovered from the reactor is composed of the lignin-derived residue and catalyst. It can be seen in Fig. 9(a) that recovered NiMoY30 loses about 45% wt. after heating up to a temperature of 500 °C. The weight loss reaches a constant value of ~ 55% and becomes independent of further increasing temperature (500–800 °C). The residues after the TGA experiment are composed of an oxidized catalyst and ash. Based on the TGA temperature profile, the recovered NiMoY30 catalyst with solid residue from the hydrotreatment experiment was regenerated by calcination in air at 450 °C for 3 h. Fig. 9 (b) compares XRD patterns of the regenerated NiMoY30 (non– sulfided) and those of the freshly synthesized, sulfided, recovered samples. The diffraction patterns show only minor differences. The peak at a 2θ value of 26.7°, corresponding to the MoO_3 phase, was found to intensify for the regenerated catalyst, similar to as it was for the original as-synthesized sample before sulfidation. This indicates some agglomeration/sintering of the MoO_3 particles formed from the MoS_2 during the regeneration in air. Using Scherrer's equation, the particle size of MoO_3 was found to increase by 8.5% after the regeneration (16.4 nm vs 17.8 nm). However, the recovered and sulfided NiMoY30 showed similar reflections of the zeolite structure demonstrating the stability of Y30 during the hydrotreatment experiments and its good potential to be regenerated.

In summary, recovered catalysts after hydrotreatment can be regenerated via simple air calcination. However, the resulting activity of the catalyst (Table S1) can be affected since it will contain inorganic impurities present from the Kraft lignin of the first run and in addition the thermal treatment can influence the catalyst, which was observed by XRD. Indeed, hydrotreatment with the regenerated catalyst showed a 20% decrease in the liquid product yield compared to the NiMoY30, but with almost no change in the solid product yield (see table S1). Other characterization results (FTIR and NMR) for the solid residue are shown in the supplementary materials.

4. Conclusions

NiMo sulfide impregnated over commercial, dealuminated and desilicated USY zeolites have been investigated in an autoclave reactor for Kraft lignin valorization. The major hurdle in obtaining a high monomer yield from one-pot hydrotreatment is to suppress the repolymerization of the reactive depolymerized fragments, which was found here to occur largely during the heating of the reactor at temperatures at which the catalysts lack sufficient hydrogenation activity. Thermal depolymerization without catalyst thus yields a high amount (47 wt%) of lignin-derived solid residue. The presence of USY zeolites, especially Y30 shows a 20% reduction in the solid residue yield due to its high surface acidity that promotes the stabilization of the lignin fragments, isomerization, and dehydration reactions and thus increases the liquid product yield. NiMo impregnated over Y30 shows an improved yield of 30.5 wt% with a high monocyclic and alkylbenzene selectivity (~61%) during the reductive hydrotreatment of Kraft lignin at 400 °C for 5 h. The solid residue yield was reduced to a value of 24 wt%. Other catalysts, mainly NiMo sulfides over dealuminated and desilicated catalysts show lower activities than NiMoY30 due mainly to lower acidity and to a lesser degree the loss of shape-selective micropores respectively.

It was also found that the liquid product yield correlated well with the total and Bronsted acidity of the catalysts, whereas the solid residue yield correlated more weakly with acidity. To further elucidate the role of impregnated NiMoY30, the catalytic activities of hydrothermally synthesized unsupported UNiMoS, and a physical mixture of UNiMoS and Y30 were compared. In terms of liquid yield, impregnated NiMoY30 and the physical mixture shows similar yield, however monocyclics and alkylbenzene selectivity drops (~30%) for the physical mixture. Solid residue with this physical mixture could be reduced further to ~ 16.7 wt % due to enhanced accessibility of the NiMoS active sites and stabilization of lignin fragments. An extended reaction time with higher catalyst loading of impregnated NiMoY30 showed remarkable monocyclics and alkylbenzene selectivity (79%) with an overall liquid product and solid yield of 38.9 wt% and 16.4 wt% respectively. Catalyst characterization revealed that the reason for this high selectivity can be ascribed to improved stabilization of monomeric fragments via catalytic hydrogen activation at a lower temperature, subsequent hydrogenation, and the hydrodeoxygenation ability of the catalyst. The proximity of the deoxygenation sites (NiMoS) and acidic sites of the catalyst was found beneficial for suppressing the formation of polycyclic aromatics as evident from their lower selectivity with NiMoS impregnated USY catalysts. However, the textural properties of the NiMoY30 probably limits the accessibility of large lignin fragments, resulting in the formation of more residual solids.

Declaration of Competing Interest

The authors declare that they have no known competing financial interests or personal relationships that could have appeared to influence the work reported in this paper.

Acknowledgments

This work is performed at the Competence Centre for Catalysis (KCK) and the Chemical Engineering division at the Chalmers University of Technology. We would like to acknowledge the Swedish Energy Agency (2017-010890, and 2018-012459), Formas (Contract: 2017-01392), and Preem AB for financial support. We would also, like to acknowledge Eric Tam, Katarina Logg, and Stefan Gustafsson from Chalmers Materials Analysis Laboratory (CMAL) for their help with XPS, FTIR, and TEM analysis.

Appendix A. Supplementary data

Supplementary data to this article can be found online at https://doi.org/10.1016/j.cej.2022.136216.

References

[1] C. Li, X. Zhao, A. Wang, G.W. Huber, T. Zhang, Catalytic transformation of lignin for the production of chemicals and fuels, Chem. Rev. 115 (21) (2015) 11559–11624, https://doi.org/10.1021/acs.chemrev.5b00155.

[2] J. Zakzeski, P.C.A. Bruijnincx, A.L. Jongerius, B.M. Weckhuysen, The catalytic valorization of lignin for the production of renewable chemicals, Chem. Rev. 110 (6) (2010) 3552–3599, https://doi.org/10.1021/cr900354u.

[3] H. Wang, H. Ruan, M. Feng, Y. Qin, H. Job, L. Luo, C. Wang, M.H. Engelhard, E. Kuhn, X. Chen, M.P. Tucker, B. Yang, One-pot process for hydrodeoxygenation of lignin to alkanes using Ru-based bimetallic and bifunctional catalysts supported on zeolite Y, ChemSusChem 10 (8) (2017) 1846–1856, https://doi.org/10.1002/cssc.201700160.

[4] R. Rinaldi, R. Jastrzebski, M.T. Clough, J. Ralph, M. Kennema, P.C. Bruijnincx, B. M. Weckhuysen, Paving the way for lignin valorisation: recent advances in bioengineering biorefining and catalysis, Angew Chem Int Ed Engl 55 (29) (2016) 8164–8215, https://doi.org/10.1002/anie.201510351.

[5] Z. Cao, M. Dierks, M.T. Clough, I.B. Daltro de Castro, R. Rinaldi, A convergent approach for a deep converting lignin-first biorefinery rendering high-energy-density drop-in Fuels, Joule 2 (6) (2018) 1118–1133, https://doi.org/10.1016/j.joule.2018.03.012.

[6] L. Dong, L. Lin, X. Han, X. Si, X. Liu, Y. Guo, F. Lu, S. Rudić, S.F. Parker, S. Yang, Y. Wang, Breaking the limit of lignin monomer production via cleavage of interunit carbon-carbon linkages, Chem 5 (6) (2019) 1521–1536, https://doi.org/10.1016/j.chempr.2019.03.007.

[7] W. Schutyser, T. Renders, S. Van den Bosch, S.F. Koelewijn, G.T. Beckham, B. F. Sels, Chemicals from lignin: an interplay of lignocellulose fractionation, depolymerisation, and upgrading, Chem. Soc. Rev. 47 (3) (2018) 852–908, https://doi.org/10.1039/c7cs00566k.

[8] Z. Sun, B. Fridrich, A. de Santi, S. Elangovan, K. Barta, Bright side of lignin depolymerization: toward new platform chemicals, Chem. Rev. 118 (2) (2018) 614–678, https://doi.org/10.1021/acs.chemrev.7b00588.

[9] P.J. de Wild, W.J. Huijgen, A. Kloekhorst, R.K. Chowdari, H.J. Heeres, Biobased alkylphenols from lignins via a two-step pyrolysis - Hydrodeoxygenation approach, Bioresour. Technol. 229 (2017) 160–168, https://doi.org/10.1016/j.biortech.2017.01.014.

[10] T. Ren, S. You, M. Zhang, Y. Wang, W. Qi, R. Su, Z. He, Improved conversion efficiency of lignin-to-fuel conversion by limiting catalyst deactivation, Chem. Eng. J. 410 (2021) 128270.

[11] A. Narani, R.K. Chowdari, C. Cannilla, G. Bonura, F. Frusteri, H.J. Heeres, K. Barta, Efficient catalytic hydrotreatment of Kraft lignin to alkylphenolics using supported NiW and NiMo catalysts in supercritical methanol, Green Chem. 17 (11) (2015) 5046–5057, https://doi.org/10.1039/c5gc01643f.

[12] J. Horáček, F. Homola, I. Kubičková, D. Kubička, Lignin to liquids over sulfided catalysts, Catal. Today 179 (1) (2012) 191–198, https://doi.org/10.1016/j.cattod.2011.06.031.

[13] K. Wu, W. Wang, H. Guo, Y. Yang, Y. Huang, W. Li, C. Li, Engineering Co Nanoparticles Supported on Defect MoS_{2-x} for Mild Deoxygenation of Lignin-Derived Phenols to Arenes, ACS Energy Lett. 5 (4) (2020) 1330–1336, https://doi.org/10.1021/acsenergylett.0c00411.

[14] W. Song, S. Zhou, S. Hu, W. Lai, Y. Lian, J. Wang, W. Yang, M. Wang, P. Wang, X. Jiang, Surface Engineering of CoMoS Nanosulfide for Hydrodeoxygenation of Lignin-Derived Phenols to Arenes, ACS Catal. 9 (1) (2018) 259–268, https://doi.org/10.1021/acscatal.8b03402.

[15] K. Wu, Y. Liu, W. Wang, Y. Huang, W. Li, Q. Shi, Y. Yang, Preparation of hydrophobic MoS_2, NiS_2-MoS_2 and CoS_2-MoS_2 for catalytic hydrodeoxygenation of lignin-derived phenols, Molecular Catalysis 477 (2019) 110537.

[16] J. Cao, A.n. Li, Y. Zhang, L. Mu, X.i. Huang, Y. Li, T. Yang, C. Zhang, C. Zhou, Highly efficient unsupported Co-doped nano-MoS2 catalysts for p-cresol hydrodeoxygenation, Molecular Catalysis 505 (2021) 111507.

[17] G. Liu, A.W. Robertson, M.-J. Li, W.C.H. Kuo, M.T. Darby, M.H. Muhieddine, Y.-C. Lin, K. Suenaga, M. Stamatakis, J.H. Warner, S.C.E. Tsang, MoS_2 monolayer catalyst doped with isolated Co atoms for the hydrodeoxygenation reaction, Nat. Chem. 9 (8) (2017) 810–816.

[18] X. Liu, X. Hou, Y. Zhang, H. Yuan, X. Hong, G. Liu, In Situ Formation of CoMoS Interfaces for Selective Hydrodeoxygenation of p-Cresol to Toluene, Ind. Eng. Chem. Res. 59 (36) (2020) 15921–15928, https://doi.org/10.1021/acs.iecr.0c03589.

[19] C. García-Mendoza, C.E. Santolalla-Vargas, L.G. Woolfolk, P. del Ángel, J.a., de los Reyes, Effect of TiO2 in supported NiWS catalysts for the hydrodeoxygenation of guaiacol, Catal. Today 377 (2021) 145–156, https://doi.org/10.1016/j.cattod.2020.08.026.

[20] W. Wang, K. Zhang, L. Li, K. Wu, P. Liu, Y. Yang, Synthesis of Highly Active Co–Mo–S Unsupported Catalysts by a One-Step Hydrothermal Method for p-Cresol Hydrodeoxygenation, Ind. Eng. Chem. Res. 53 (49) (2014) 19001–19009, https://doi.org/10.1021/ie5032698.

[21] E.L.a.B. Delmon, Influence of Oxygen-, Nitrogen-, and Sulfur-Containing Compounds on the Hydrodeoxygenation of Phenols over Sulfided CoMo/y-Al_2O_3 and NiMo/y-Al_2O_3 Catalysts, Ind. Eng. Chem. Res. 32 (1993) 2516-2524.

[22] M. Koyama, Hydrocracking of lignin-related model dimers, Bioresour. Technol. 44 (1993) 209–215, https://doi.org/10.1016/0960-8524(93)90154-4.

[23] L. Shuai, J. Sitison, S. Sadula, J. Ding, M.C. Thies, B. Saha, Selective C-C Bond Cleavage of Methylene-Linked Lignin Models and Kraft Lignin, ACS Catal. 8 (7) (2018) 6507–6512, https://doi.org/10.1021/acscatal.8b00200.

[24] W. Song, W. Lai, Y. Lian, X. Jiang, W. Yang, Sulfated ZrO_2 supported CoMo sulfide catalyst by surface exsolution for enhanced hydrodeoxygenation of lignin-derived ethers to aromatics, Fuel 263 (2020) 116705.

[25] C. Zhang, J. Lu, X. Zhang, K. MacArthur, M. Heggen, H. Li, F. Wang, Cleavage of the lignin β-O-4 ether bond via a dehydroxylation–hydrogenation strategy over a NiMo sulfide catalyst, Green Chem. 18 (24) (2016) 6545–6555, https://doi.org/10.1039/c6gc01456a.

[26] C. Zhang, H. Li, J. Lu, X. Zhang, K.E. MacArthur, M. Heggen, F. Wang, Promoting Lignin Depolymerization and Restraining the Condensation via an Oxidation−Hydrogenation Strategy, ACS Catal. 7 (5) (2017) 3419–3429, https://doi.org/10.1021/acscatal.7b00148.

[27] N. Ji, X. Wang, C. Weidenthaler, B. Spliethoff, R. Rinaldi, Iron(II) Disulfides as Precursors of Highly Selective Catalysts for Hydrodeoxygenation of Dibenzyl Ether into Toluene, ChemCatChem 7 (6) (2015) 960–966, https://doi.org/10.1002/cctc.201500041.

[28] C. Sepúlveda, R. García, P. Reyes, I.T. Ghampson, J.L.G. Fierro, D. Laurenti, M. Vrinat, N. Escalona, Hydrodeoxygenation of guaiacol over ReS2/activated carbon catalysts. Support and Re loading effect, Appl. Catal., A 475 (2014) 427–437, https://doi.org/10.1016/j.apcata.2014.01.057.

[29] Q. Tian, N. Li, J. Liu, M. Wang, J. Deng, J. Zhou, Q. Ma, Catalytic Hydrogenation of Alkali Lignin to Bio-oil Using Fullerene-like Vanadium Sulfide, Energy Fuels 29 (1) (2014) 255–261, https://doi.org/10.1021/ef502244t.

[30] B. Yoosuk, D. Tumnantong, P. Prasassarakich, Unsupported MoS_2 and $CoMoS_2$ catalysts for hydrodeoxygenation of phenol, Chem. Eng. Sci. 79 (2012) 1–7, https://doi.org/10.1016/j.ces.2012.05.020.

[31] D. Kubička, J. Horáček, Deactivation of HDS catalysts in deoxygenation of vegetable oils, Appl. Catal. A 394 (1-2) (2011) 9–17.

[32] J. Pu, T.-S. Nguyen, E. Leclerc, C. Lorentz, D. Laurenti, I. Pitault, M. Tayakout-Fayolle, C. Geantet, Lignin catalytic hydroconversion in a semi-continuous reactor: An experimental study, Applied Catalysis B-Environmental 256 (2019) 117769.

[33] S. Mukundan, D. Boffito, A. Shrotri, L. Atanda, J. Beltramini, G. Patience, Thermocatalytic Hydrodeoxygenation and Depolymerization of Waste Lignin to Oxygenates and Biofuels in a Continuous Flow Reactor at Atmospheric Pressure, ACS Sustainable Chem. Eng. 8 (35) (2020) 13195–13205, https://doi.org/10.1021/acssuschemeng.0c02102.

[34] S. Mukundan, L. Atanda, J. Beltramini, Thermocatalytic cleavage of C-C and C–O bonds in model compounds and kraft lignin by NiMoS2/C nanocatalysts, Sustainable Energy Fuels 3 (5) (2019) 1317–1328, https://doi.org/10.1039/c8se00576a.

[35] A. Oasmaa, R. Alén, D. Meier, Catalytic hydrotreatment of some technical lignins, Bioresour. Technol. 45 (3) (1993) 189–194.

[36] D. Meier, R. Ante, O. Faix, Catalytic hydropyrolysis of lignin: Influence of reaction conditions on the formation and composition of liquid products, Bioresour. Technol. 40 (2) (1992) 171–177.

[37] C.R. Kumar, N. Anand, A. Kloekhorst, C. Cannilla, G. Bonura, F. Frusteri, K. Barta, H.J. Heeres, Solvent free depolymerization of Kraft lignin to alkyl-phenolics using supported NiMo and CoMo catalysts, Green Chem. 17 (11) (2015) 4921–4930, https://doi.org/10.1039/c5gc01641j.

[38] S. Liu, A.P. van Muyden, L. Bai, X. Cui, Z. Fei, X. Li, X. Hu, P.J. Dyson, Metal-Sulfide Catalysts Derived from Lignosulfonate and their Efficient Use in Hydrogenolysis, ChemSusChem 12 (14) (2019) 3271–3277, https://doi.org/10.1002/cssc.201900677.

[39] N. Li, L. Wei, R. bibi, L. Chen, J. Liu, L.i. Zhang, Y. Zheng, J. Zhou, Catalytic hydrogenation of alkali lignin into bio-oil using flower-like hierarchical MoS_2 -based composite catalysts, Fuel 185 185 (2016) 532–540.

[40] Z. Ma, E. Troussard, J.A. van Bokhoven, Controlling the selectivity to chemicals from lignin via catalytic fast pyrolysis, Appl. Catal. A 423-424 (2012) 130–136.

[41] J. Garcia-Martinez, K. Li, G. Krishnaiah, A mesostructured Y zeolite as a superior FCC catalyst–lab to refinery, Chem Commun (Camb) 48 (97) (2012) 11841–11843, https://doi.org/10.1039/c2cc35659g.

[42] S. Abdulridha, Y. Jiao, S. Xu, R. Zhang, Z. Ren, A.A. Garforth, X. Fan, A,, in: Comparative Study on Mesoporous Y Zeolites Prepared by Hard-Templating and Post-Synthetic Treatment Methods, 2021, p. 612, https://doi.org/10.1016/j.apcata.2020.117986.

[43] Z. Ma, J.A. van Bokhoven, Deactivation and Regeneration of H-USY Zeolite during Lignin Catalytic Fast Pyrolysis, ChemCatChem 4 (12) (2012) 2036–2044, https://doi.org/10.1002/cctc.201200401.

[44] A.K. Deepa, P.L. Dhepe, Solid acid catalyzed depolymerization of lignin into value added aromatic monomers, RSC, Advances 4 (25) (2014) 12625.

[45] P. Sirous-Rezaei, Y.-K. Park, Catalytic hydropyrolysis of lignin: Suppression of coke formation in mild hydrodeoxygenation of lignin-derived phenolics, Chem. Eng. J. 386 (2020) 121348.

[46] M. Grilc, B. Likozar, J. Levec, Simultaneous Liquefaction and Hydrodeoxygenation of Lignocellulosic Biomass over NiMo/Al_2O_3, Pd/Al_2O_3, and Zeolite Y Catalysts in Hydrogen Donor Solvents, ChemCatChem 8 (1) (2016) 180–191, https://doi.org/10.1002/cctc.201500840.

[47] N.C. Baxter, Y. Wang, H. Huang, Y. Liao, H. Barnett, Y. Zhao, S. Wang, Kraft Lignin Ethanolysis over Zeolites with Different Acidity and Pore Structures for Aromatics Production, Catalysts 11 (2) (2021), https://doi.org/10.3390/catal11020270.

[48] M.A. Salam, P. Arora, H. Ojagh, Y.W. Cheah, L. Olsson, D. Creaser, NiMoS on alumina-USY zeolites for hydrotreating lignin dimers: effect of support acidity and cleavage of C-C bonds, Sustainable Energy Fuels 4 (1) (2020) 149–163, https://doi.org/10.1039/c9se00507b.

[49] M.A. Salam, Y.W. Cheah, P.H. Ho, L. Olsson, D. Creaser, Hydrotreatment of lignin dimers over NiMoS-USY: effect of silica/alumina ratio, Sustainable Energy Fuels 5 (13) (2021) 3445–3457, https://doi.org/10.1039/d1se00412c.

[50] B.M. Santos, W. Zhao, J.L. Zotin, M.A.P.d. Silva, L. Oliviero, F. Maugé, Impact of proximity between NiMoS and zeolitic HY sites on cyclohexene hydroconversion: An infrared operando study of sulfide catalysts, J. Catal. 396 (2021) 92–103.

[51] P.M. Train, M.T. Klein, Hydroprocessing lignin and lignin model compounds: Products, kinetics, and catalyst aging, Fuel Sci. Technol. Int. 9 (2) (1991) 193–227.

[52] P.H. Ho, J. Woo, R.F. Ilmasani, M.A. Salam, D. Creaser, L. Olsson, The Effect of Si/Al Ratio on the Oxidation and Sulfur Resistance of Beta Zeolite-Supported Pt and Pd as Diesel Oxidation Catalysts, ACS Engineering Au 2 (1) (2022) 27–45.
[53] Y.W. Cheah, M.A. Salam, P. Arora, O. Öhrman, D. Creaser, L. Olsson, Role of transition metals on MoS2-based supported catalysts for hydrodeoxygenation (HDO) of propylguaiacol, Sustainable Energy Fuels 5 (7) (2021) 2097–2113, https://doi.org/10.1039/d1se00184a.
[54] Q. Yan, J. Li, J. Zhang, Z. Cai, Thermal Decomposition of Kraft Lignin under Gas Atmospheres of Argon, Hydrogen, and Carbon Dioxide, Polymers 10 (7) (2018), https://doi.org/10.3390/polym10070729.
[55] T. Belkheiri, S.-I. Andersson, C. Mattsson, L. Olausson, H. Theliander, L. Vamling, Hydrothermal Liquefaction of Kraft Lignin in Subcritical Water: Influence of Phenol as Capping Agent, Energy Fuels 32 (5) (2018) 5923–5932, https://doi.org/10.1021/acs.energyfuels.8b00068.
[56] V.M. Roberts, V. Stein, T. Reiner, A. Lemonidou, X. Li, J.A. Lercher, Towards quantitative catalytic lignin depolymerization, Chemistry 17 (21) (2011) 5939–5948, https://doi.org/10.1002/chem.201002438.
[57] P.M. Mortensen, J.-D. Grunwaldt, P.A. Jensen, K.G. Knudsen, A.D. Jensen, A review of catalytic upgrading of bio-oil to engine fuels, Appl. Catal. A 407 (1-2) (2011) 1–19.
[58] C. Dupont, R. Lemeur, A. Daudin, P. Raybaud, Hydrodeoxygenation pathways catalyzed by MoS_2 and NiMoS active phases: A DFT study, J. Catal. 279 (2) (2011) 276–286, https://doi.org/10.1016/j.jcat.2011.01.025.
[59] P. Arora, H. Ojagh, J. Woo, E. Lind Grennfelt, L. Olsson, D. Creaser, Investigating the effect of Fe as a poison for catalytic HDO over sulfided NiMo alumina catalysts, Appl. Catal., B 227 (2018) 240–251, https://doi.org/10.1016/j.apcatb.2018.01.027.
[60] M. Sun, A. Nelson, J. Adjaye, Ab initio DFT study of hydrogen dissociation on MoS_2, NiMoS, and CoMoS: mechanism, kinetics, and vibrational frequencies, J. Catal. 233 (2) (2005) 411–421, https://doi.org/10.1016/j.jcat.2005.05.009.
[61] F. Cheng, C.E. Brewer, Producing jet fuel from biomass lignin: Potential pathways to alkyl-benzenes and cycloalkanes, Renew. Sustain. Energy Rev. 72 (2017) 673–722, https://doi.org/10.1016/j.rser.2017.01.030.
[62] J. Weitkamp, Catalytic Hydrocracking-Mechanisms and Versatility of the Process, ChemCatChem 4 (3) (2012) 292–306, https://doi.org/10.1002/cctc.201100315.
[63] M. Oregui-Bengoechea, I. Gandarias, N. Miletić, S.F. Simonsen, A. Kronstad, P. L. Arias, T. Barth, Thermocatalytic conversion of lignin in an ethanol/formic acid medium with NiMo catalysts: Role of the metal and acid sites, Appl. Catal., B 217 (2017) 353–364, https://doi.org/10.1016/j.apcatb.2017.06.004.
[64] Y.W. Cheah, M.A. Salam, J. Sebastian, S. Ghosh, O. Öhrman, D. Creaser, L. Olsson, Thermal annealing effects on hydrothermally synthesized unsupported MoS2 for enhanced deoxygenation of Propylguaiacol and Kraft lignin, Sustainable Energy Fuels 5 (20) (2021) 5270–5286.
[65] Y. Zhang, F. Lu, L. Pan, Y. Xu, Y. Yang, Y. Bando, D. Golberg, J. Yao, X. Wang, Improved cycling stability of NiS2 cathodes through designing a “kiwano” hollow structure, J. Mater. Chem. A 6 (25) (2018) 11978–11984, https://doi.org/10.1039/c8ta01551a.
[66] M. Chhowalla, G.A.J. Amaratunga, Thin films of fullerene-like MoS_2 nanoparticles with ultra-low friction and wear, Nature 407 (6801) (2000) 164–167.
[67] L. Yang, X. Cui, J. Zhang, K. Wang, M. Shen, S. Zeng, S.A. Dayeh, L. Feng, B. Xiang, Lattice strain effects on the optical properties of MoS2 nanosheets, Sci Rep 4 (2014) 5649, https://doi.org/10.1038/srep05649.
[68] W. Wang, L. Li, K. Wu, K. Zhang, J. Jie, Y. Yang, Preparation of Ni–Mo–S catalysts by hydrothermal method and their hydrodeoxygenation properties, Appl. Catal., A 495 (2015) 8–16, https://doi.org/10.1016/j.apcata.2015.01.041.
[69] D. Verboekend, G. Vilé, J. Pérez-Ramírez, Hierarchical Y and USY Zeolites Designed by Post-Synthetic Strategies, Adv. Funct. Mater. 22 (5) (2012) 916–928, https://doi.org/10.1002/adfm.201102411.
[70] D. Verboekend, G. Vilé, J. Pérez-Ramírez, Mesopore Formation in USY and Beta Zeolites by Base Leaching: Selection Criteria and Optimization of Pore-Directing Agents, Cryst. Growth Des. 12 (6) (2012) 3123–3132, https://doi.org/10.1021/cg3003228.
[71] M. Gackowski, K. Tarach, Ł. Kuterasiński, J. Podobiński, S. Jarczewski, P. Kuśtrowski, J. Datka, Hierarchical zeolites Y obtained by desilication: Porosity, acidity and catalytic properties, Microporous Mesoporous Mater. 263 (2018) 282–288, https://doi.org/10.1016/j.micromeso.2017.11.051.
[72] D. Verboekend, N. Nuttens, R. Locus, J. Van Aelst, P. Verolme, J.C. Groen, J. Perez-Ramirez, B.F. Sels, Synthesis, characterisation, and catalytic evaluation of hierarchical faujasite zeolites: milestones, challenges, and future directions, Chem. Soc. Rev. 45 (12) (2016) 3331–3352, https://doi.org/10.1039/c5cs00520e.
[73] X. Xi, F. Zeng, H. Cao, C. Cannilla, T. Bisswanger, S. de Graaf, Y. Pei, F. Frusteri, C. Stampfer, R. Palkovits, H.J. Heeres, Enhanced C3+ alcohol synthesis from syngas using KCoMoSx catalysts: effect of the Co-Mo ratio on catalyst performance, Appl. Catal., B 272 (2020) 118950.
[74] F. Labruyère, M. Lacroix, D. Schweich, M. Breysse, High-pressure temperature-programmed reduction of sulfided catalysts, J. Catal. 167 (2) (1997) 464–469, https://doi.org/10.1006/jcat.1997.1602.
[75] C. Zhang, K. Liu, Y. Zhang, L. Mu, Z. Zhang, J. Huang, Y. Wang, T. Yang, J. Cao, C. Zhou, Co-promoted few-layer and defect-rich MoS2 for enhanced hydrodeoxygenation of p-cresol, Appl. Catal., A 621 621 (2021) 118175.
[76] M.F. Wagenhofer, H. Shi, O.Y. Gutiérrez, A. Jentys, J.A. Lercher, Enhancing hydrogenation activity of Ni-Mo sulfide hydrodesulfurization catalysts, Science, Advances 6 (19) (2020) eaax5331, https://doi.org/10.1126/sciadv.aax5331.
[77] F. Vogelgsang, Y. Ji, H. Shi, J.A. Lercher, On the multifaceted roles of NiSx in hydrodearomatization reactions catalyzed by unsupported Ni-promoted MoS_2, J. Catal. 391 (2020) 212–223, https://doi.org/10.1016/j.jcat.2020.08.026.
[78] S. Eijsbouts, X. Li, J. Bergwerff, J. Louwen, L. Woning, J. Loos, Nickel sulfide crystals in Ni-Mo and Ni-W catalysts: Eye-catching inactive feature or an active phase in its own right? Catal. Today 292 (2017) 38–50, https://doi.org/10.1016/j.cattod.2016.08.028.